Univerzita Karlova v Praze

Matematicko-fyzikální fakulta

BAKALÁŘSKÁ PRÁCE

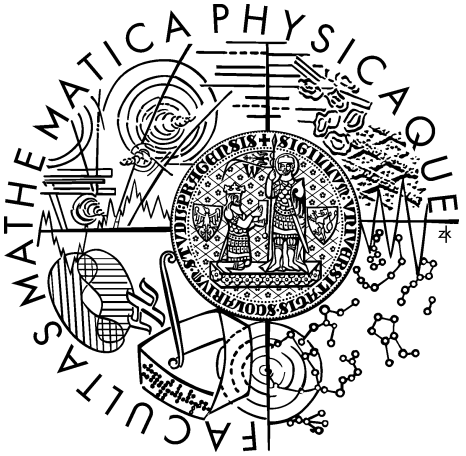

Tereza Perlácová

Matematické modely pro nestlačitelné nenewtonovské tekutiny s nemonotónní závislostí smykového napětí na rychlosti smyku

Matematický ústav UK

Vedoucí bakalářské práce: Mgr. Vít Průša, Ph.D.

Studijní program: Obecná fyzika

Praha 2014

Charles University in Prague

Faculty of Mathematics and Physics

BACHELOR THESIS

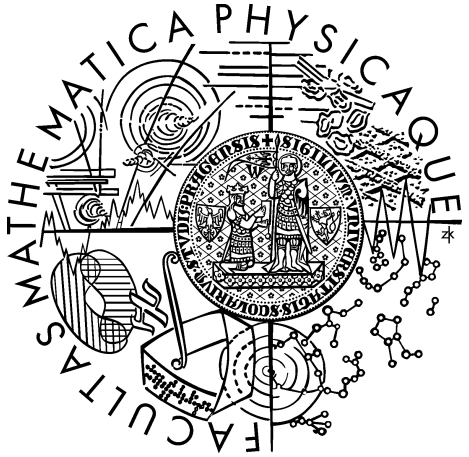

Tereza Perlácová

Mathematical models for incompressible non-newtonian fluids with non-monotone dependence of shear stress on shear rate

Mathematical Institute of Charles University

Supervisor of the bachelor thesis: Mgr. Vít Průša, Ph.D.

Study programme: General Physics

Prague 2014

Acknowledgements

I would like to express my sincere gratitude to my bachelor thesis supervisor, Mgr. Vít Průša, Ph.D. for his patient guidance, willingness and helpful advice during the work on the thesis. Also, I would like to thank my family for their persistent help and encouragement during all my studies.

I declare that I carried out this bachelor thesis independently, and only with the cited sources, literature and other professional sources.

I understand that my work relates to the rights and obligations under the Act No. 121/2000 Coll., the Copyright Act, as amended, in particular the fact that the Charles University in Prague has the right to conclude a license agreement on the use of this work as a school work pursuant to Section 60 paragraph 1 of the Copyright Act.

In Prague May 21, 2014 signature of the author

Název práce: Matematické modely pro nestlačitelné nenewtonovské tekutiny s nemonotónní závislostí smykového napětí na rychlosti smyku

Autor: Tereza Perlácová

Katedra: Matematický ústav UK

Vedoucí bakalářské práce: Mgr. Vít Průša, Ph.D.

Abstrakt: Práca skúma rozvíjajúcu sa teóriu, ktorá zavádza implicitné konštitutívne vzťahy do modelovania tekutín. Vychádzame z podrobnej rešerše vedeckej literatúry, ktorá je zameraná na experimentálne data závislosti šmykového napätia na rýchlosti šmyku v tvare písmena S. Nájdené materiály, ktoré vykazujú tento typ správania sú koloidálne suspenzie a tenzidové roztoky. Práca zhrňuje mikroskopické teórie, ktoré vysvetľujú procesy nárastu a poklesu viskozity týchto materiálov s rastúcou rýchlosťou šmyku a proces vzniku pásov indukovaných šmykom. Na základe týchto teórií tvrdíme, že v prípade meraní s kontrolovaným napätím je atypické správanie spôsobené separáciou tekutiny na niekoľko pásov. Nájdené experimentálne data sme nafitovali niekoľkými navrhnutými jednodimenzionálnymi vzťahmi, ktoré sú zahrnuté v triede implicitných konštitutívnych vzťahov. Na záver sme navrhli príklad implicitného, plne trojdimenzionálneho konštitutívneho vzťahu s ohľadom na efekt rozdielu normálových napätí. Práca tak celkovo demonštruje prínos implicitnej konštitutívnej teórie pre modelovanie komplexných tekutín.

Klíčová slova: nestlačiteľné nenewtonovské tekutiny, implicitná konštitutívná teória, rozdiel normálových napätí, experimentálne data

Title: Mathematical models for incompressible non-newtonian fluids with non-monotone dependence of shear stress on shear rate

Author: Tereza Perlácová

Department: Mathematical institute of Charles University

Supervisor: Mgr. Vít Průša, Ph.D.

Abstract: We investigate recently developed implicit constitutive theory and its implication into the modelling of fluids. We base the work on the literature search that is focused on the S-shaped shear stress-shear rate experimental data. The materials that exhibit such a behavior are found to be colloidal suspensions and surfactant solutions. The work summarizes microscopical theories explaining the shear-thickening, the shear-thinning and the shear-banding phenomena that arise in these materials. The theories reveal that the unusual behavior is due to the separation of the fluid into various bands in shear stress-controlled measurements. The extracted experimental data from the literature are fitted with several one-dimensional implicit type relations. Finally, we propose an example of a fully three-dimensional implicit constitutive relation with focus on the normal stress differences effect. The work demonstrates benefits of the implicit constitutive theory for modelling of complex fluids.

Keywords: incompressible nonnewtonian fluids, implicit constitutive theory, normal stress differences, experimental data

Contents

Introduction

Implicit constitutive relations

The response of the majority of fluid like materials to the applied stresses is typically described by the constitutive relation in the form

$$\mathbb{T}_\delta = f(\mathbb{D}), \tag{1}$$

where $\mathbb{T}_\delta$ is the traceless part of the Cauchy stress tensor, $\mathbb{D}$ is the symmetric part of the velocity gradient and f is a tensorial function. Water flow in a pipe, air flow around a wing, blood flow in the arteries or the highly shear-thickening liquid gel used in bulletproof vests, all of these examples of the fluid flow can be modelled with relations of the type (1) and serve therefore as the illustration of their vast use.

Due to their form, constitutive relations of the type (1) are referred to as explicit constitutive relations. They express explicitly the stress in terms of the kinematic quantities that are independent variables of the function f. A generalization of (1) is a class of implicit relations

$$g(\mathbb{T}_\delta, \mathbb{D}) = \mathbb{0}, \tag{2}$$

where g is a tensorial function. Obviously, the class of relations (1) represents a subclass of the implicit relations (2). These can however take an important number of other explicit forms, for example

$$\mathbb{D} = h(\mathbb{T}_\delta), \tag{3}$$

where h is a tensorial function. In the class of relations (3), kinematic quantities (the effect) are expressed as a function of the stress (the cause). In comparison with classical constitutive relations (1), the relations (3) provide another approach to the modelling of material response.

The use of the implicit constitutive theory could therefore bring a new viewpoint on the modelling of material responses. The principal benefit of its introduction into the mathematical modelling is clearly expressed in the work Rajagopal (2003). Rajagopal, one of the first who introduced the systematical approach of the theory of implicit relations, claims that the new framework on the relations *allows one to bring under one unifying theme a much richer and wider class of material response.* The framework of implicit constitutive relations have been further developed during the last years in many scientific publications such as Málek et al. (2010), Průša and Rajagopal (2012) or Rajagopal and Srinivasa (2008).

Objectives

Our work is organized so that it fulfills two principal objectives.

The first of them is to demonstrate the need of the implicit constitutive theory for

the description of some fluid behavior. To do so, we will perform a complex literature search focused on the material responses that have a common feature: they are described by an S-shaped shear stress-shear rate curve. The found experimental data will be fitted by suitable one-dimensional relations stemming from the implicit constitutive theory.

Our second objective is to construct an example of constitutive relation of the implicit type. A systematical procedure of construction will lead us to a full three-dimensional constitutive relation that will satisfy the required admissibility conditions.

1. Governing equations and constitutive relations in continuum mechanics

The objective of this section is to introduce the basic principles of the fluid mechanics and to introduce the useful notation used in the rest of the work.

In the theory of mechanics, fluid is treated in two different ways.

In the first approach, the fluid is considered as the system of discrete units: molecules composed of atoms and those in turn of subatomic particles. These structural units interact with each other and their behavior is related to the macroscopic physical properties of the whole system such as viscosity, pressure and volume. If one is interested in these properties, one has to solve the system of equations that relate them with the molecular behavior. The complicated nature of the equations and the lack of basic molecular data make however the solution of the corresponding system practically unfeasible and one naturally tends to prefer the measurement of the macroscopic properties. Particularly for a large number of the structural units, this approach of the fluid is highly unpractical.

As a much more useful and applicable approach to the mathematical modeling of the fluid motion seems to be the concept of continuous media. The continuum is considered as composed of an infinity of material points and matter is interpreted as the continuously distributed quantity. This approach postulates that macroscopic properties are ascribed to each point and that they are distributed continuously, see Schowalter (1978).

Generally, if one wants to describe the evolution of a rigid body, one solves the equations relating its motion to the applied forces, known as Newton's laws. In the theory of continuum, the procedure is analogical. However, to describe the temporal evolution of a continuum, one uses the laws in a different, more appropriate form. In analogy to the Newton's and the related conservation laws, continuum mechanics formulates a set of balance (or governing) equations.

1.1 Governing equations in Eulerian description

The governing equations in continuum mechanics are partial differential equations that describe the behavior and the temporal evolution of a system. From another perspective, we can consider them as the counterparts of conservation laws that are formulated for rigid or point particles.

We define the governing equations for a domain $\Omega \subset \mathbb{R}^3$ occupied by the fluid for which we prescribe initial and boundary conditions. The fluid motion is expressed in

the so called Eulerian description that is based on the determination of the velocity field $\mathbf{v}(\mathrm{x},\ \mathrm{t}) = (v_1(\mathrm{x,t}),\ v_2(\mathrm{x,t}),\ v_3(\mathrm{x,t}))$ and other quantities at given spatial point x and time t.

We will adopt the following notation: ρ - the density of fluid, p - pressure, $\mathbf{v}$ - velocity in the Eulerian description and t - time.

1.1.1 General material

The following equations are valid for any material as long as we are willing to model the material as continuous medium.

- The continuity equation - law of conservation of mass

$$\frac{\partial \rho}{\partial t} + \operatorname{div}(\rho \mathbf{v}) = 0. \tag{1.1}$$

- The equations of motion - law of conservation of momentum

$$\frac{\partial}{\partial t}(\rho \mathbf{v}) + \operatorname{div}(\rho \mathbf{v} \otimes \mathbf{v}) = \rho \mathbf{f} + \operatorname{div}\mathbb{T}, \tag{1.2}$$

  $\mathbf{v} \otimes \mathbf{v}$ is the tensor with components $v_i v_j$, $i, j \in \{1, 2, 3\}$; $\mathbf{f}$ is the body force and $\mathbb{T}$ is the Cauchy stress tensor.

- The law of conservation of angular momentum
  This law is in the absence of internal couples equivalent to the relation

$$\mathbb{T} = \mathbb{T}^{\top}. \tag{1.3}$$

- The energy equation - law of conservation of energy

$$\frac{\partial E}{\partial t} + \operatorname{div}(E\mathbf{v}) = \rho \mathbf{f} \cdot \mathbf{v} + \operatorname{div}(\mathbb{T}\mathbf{v}) + \rho q - \operatorname{div}\mathbf{q}, \tag{1.4}$$

  where the total energy E is expressed as $E = \rho(e + |\mathbf{v}|^2/2)$;
  q is the density of heat sources, $\mathbf{q}$ is the heat flux and e is the internal energy of the system.

1.1.2 Incompressible fluid

A homogeneous incompressible fluid is characterized by the constant density ρ in time and space. Assuming this condition, the equations (1.1) and (1.2) take the following simplified forms:

- The continuity equation

$$\operatorname{div} \mathbf{v} = 0. \tag{1.5}$$

- The equations of motion

$$\rho \frac{\mathrm{d}\mathbf{v}}{\mathrm{d}t} = \mathrm{div}\,\mathbb{T} + \rho\mathbf{b}, \tag{1.6}$$

where

$$\frac{\mathrm{d}\mathbf{v}}{\mathrm{d}t} = \frac{\partial \mathbf{v}}{\partial t} + (\mathbf{v}\cdot\nabla)\,\mathbf{v} \tag{1.7}$$

is the material time derivative.

Since the fluids we consider in this work are assumed to be incompressible, we are allowed to use the simplified forms of the balance equations.

1.2 Constitutive relations

The classical problem studied in continuum mechanics is the determination of the velocity and stress field in the domain Ω occupied by the fluid. If we assume that the fluid is incompressible, the principal tools we use for the solution of the problem are the governing equations (1.5) and (1.6) with the prescribed initial and boundary conditions. Since the density and the body force are typically known, the components of the velocity vector and of the Cauchy stress tensor are the only unknowns of the problem. In particular, we have three components of the velocity vector and six components of the stress tensor that make together *nine unknown parameters.* We have however only *four equations* (1.5) and (1.6) available. Mechanics of continuum solves this problem by the introduction of additional equations that describe the behavior of the material of interest. In particular we define a relation between the Cauchy stress tensor and the symmetric part of velocity gradient named a constitutive relation. One of the most frequently used constitutive relations is the Navier-Stokes relation,

$$\mathbb{T} = -p\mathbb{I} + 2\mu\mathbb{D}, \tag{1.8}$$

where $\mathbb{D}$ denotes the symmetric part of the velocity gradient. If we define the traceless part of the Cauchy stress tensor $\mathbb{T}_\delta$ as

$$\mathbb{T}_\delta = \mathbb{T} - \frac{1}{3}(\mathrm{Tr}\,\mathbb{T})\mathbb{I}, \tag{1.9}$$

where $\mathrm{Tr}\,\mathbb{T}$ is the trace of the tensor $\mathbb{T}$, we obtain the relation (1.8) in the form

$$\mathbb{T}_\delta = 2\mu\mathbb{D}. \tag{1.10}$$

As it can be seen in (1.8) or (1.10), the Navier-Stokes relation represents a model for the linear response of the material to the applied stress. However, fluids show in general a more complex behavior. The non-linear response of the fluid to the stress is typical for non-Newtonian fluids and the corresponding constitutive relation is classically expressed in the form

$$\mathbb{T}_\delta = f(\mathbb{D}), \tag{1.11}$$

where f is a tensorial function. The relation can also be viewed as the generalization of the linear response in (1.10).

Most of the fluids typically studied in experiments exhibit the behavior that can be described by (1.11) where the stress tensor is expressed in terms of the symmetric part of the velocity gradient. In this sense, (1.11) is an explicit constitutive relation. Less studied is the class of implicit relations

$$f(\mathbb{T}_\delta, \mathbb{D}) = 0, \tag{1.12}$$

that have been firstly systematically studied by Rajagopal (2003). This type is more general, hence it can be applied to a much wider range of materials than the classically used form (1.11). Study of constitutive relations of the type (1.12) constitutes the objective of our work.

1.3 Simple shear flow

One of the simplest geometries used in the modelling of a fluid flow is represented in Figure 1.1. In this configuration, the fluid is placed in the gap between two parallel plates that are separated by the distance of $2h$. The simplicity of this geometry rests on the specific orientation of the velocity vector $\mathbf{v}$. That leads to simple formulae for the velocity gradient $\nabla \boldsymbol{v}$, its symmetric part $\mathbb{D}$ and the Cauchy stress tensor $\mathbb{T}$.

Following the situation presented in Figure 1.1, the velocity vector has the components

$$\mathbf{v} = \left[0, 0, v^{\hat{z}}(y)\right] \tag{1.13}$$

For $y = h$, $v^{\hat{z}}$ takes the value of v_{top} and for $y = -h$, $v^{\hat{z}}$ equals to 0.

The velocity gradient then takes the form

$$\nabla \boldsymbol{v} = \begin{bmatrix} 0 & 0 & 0 \\ 0 & 0 & 0 \\ 0 & \frac{\mathrm{d}v^{\hat{z}}}{\mathrm{d}y} & 0 \end{bmatrix}. \tag{1.14}$$

If we denote $\dot{\gamma} = \frac{\mathrm{d}v^{\hat{z}}}{\mathrm{d}y}$, the symmetric part of the velocity gradient can be written as

$$\mathbb{D} = \frac{1}{2}\begin{bmatrix} 0 & 0 & 0 \\ 0 & 0 & \dot{\gamma} \\ 0 & \dot{\gamma} & 0 \end{bmatrix}. \tag{1.15}$$

The quantity $\dot{\gamma}$ is in our work referred to as the shear rate.

We assume the stress tensor in the form

$$\mathbb{T} = \begin{bmatrix} \mathrm{T}_{\hat{x}\hat{x}} & 0 & 0 \\ 0 & \mathrm{T}_{\hat{y}\hat{y}} & \sigma \\ 0 & \sigma & \mathrm{T}_{\hat{z}\hat{z}} \end{bmatrix}, \tag{1.16}$$

where we adopt for simplicity the notation $\sigma = \mathrm{T}_{\hat{y}\hat{z}} = \mathrm{T}_{\hat{z}\hat{y}}$ and we refer to σ as the shear stress. Furthermore we define the ratio

$$\eta = \frac{\sigma}{\dot{\gamma}} \tag{1.17}$$

and we refer to it as the apparent viscosity of the material.

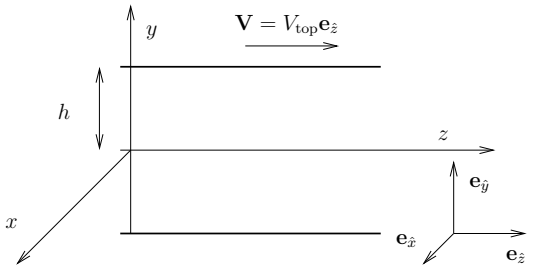

Figure 1.1: Simple shear flow geometry.

The simple shear flow geometry is the prototype of experimental settings that are used in the rheometry. The rheometrical measurements reduce usually to the finding of the relation between the shear stress σ and the shear rate $\dot{\gamma}$. Consequently the rheometrical measurements essentially give only a one dimensional relation between the particular components of the Cauchy stress tensor and the symmetric part of the velocity gradient. Hence the three-dimensional relation (1.11) or (1.12) must be abstracted from these data. Naturally, the extension of the one-dimensional relation $\sigma = f(\dot{\gamma})$ or $g(\sigma, \dot{\gamma}) = 0$ to the three-dimensional relation (1.11) or (1.12) is not unique.

2. Experimental data

The objective of this section is to present the results of our literature search. Our aim has been to find experimental data for which the dependence of the shear stress σ on the shear rate $\dot{\gamma}$ cannot be descibed by the classical type of constitutive relation $\sigma = f(\dot{\gamma})$ but one has to use the implicit form $g(\sigma, \dot{\gamma}) = 0$.

The results of our search are summarized in Table 2.1.

Material	Reference; Figure	Content of the referential work
COLLOIDAL SUSPENSIONS		
BiOCl/polyelectrolyte solution	Bertrand et al. (2002); Figure 2.1a	stress-controlled viscosity measurements, shear thickening/jamming occurence depending on the volume fraction, suggested concept of the relation between the phenomena
SURFACTANT SOLUTIONS		
TTAA/NaSal, water	Boltenhagen et al. (1997b); Figure 2.2a	stress-controlled and shear rate-controlled measurements, study of shear-flow-induced transitions present in both types
	Hu et al. (1998a); Figure 2.3a	stress-controlled and shear rate-controlled measurements, visualization of shear induced structures using laser light scattering technique, identification of various flow phases
	Hu et al. (1998b); Figure 2.4a	stress-controlled and shear rate-controlled measurements, velocity profile measurements, focus on the the behavior in the shear-thickened state
CTAT, water	Macias et al. (2001); Figure 2.5a	stress-controlled and shear rate-controlled measurements, experiment with solutions of various weight percent and performed in various rheometrical geometries, focus on the shear induced structures formation

Material	Reference; Figure	Content of the referential work
TDPS/SDS, brine	Lopez-Diaz et al. (2010); Figure 2.6a	stress-controlled and shear rate-controlled measurements, up-shear and down-shear rate measurements, experiments under various conditions: surfactant concentration, temperature and ratio of the two included surfactants
SDS/dodecane/ pentanol, water	Roux et al. (1993); Figure 2.7a	stress-controlled measurements, study of the nature of transitions between lamellar and onionlike phases for lyotropic lamellar solutions under shear
	Wilkins and Olmsted (2006); Figure 2.8a	stress-controlled measurements, vorticity banding in the lamellar-to-onion transition

Table 2.1: Materials that were found to exhibit an S-shaped shear stress - shear rate dependence. The reference with the particular experimental data and the corresponding figure in this work.

In Table 2.2 we present some other types of surfactant solutions studied in the literature. The presented scientific works are focused on the study of various aspects of the solution behavior under shear.

Material	Reference	Content
CTAB/NaSal, water	Hartmann and Cressely (1997)	viscosity measurements for different concentrations of added anions such as F^-, Cl^-, Br^-, NO_3^-
	Liu and Pine (1996)	observation of shear induced structures by light scattering measurements in the shear flow
	Dehmoune et al. (2009)	rheological study of three solutions of cationic surfactant CTAB with different length of hydrophobic part, influence of the solvent nature on the shear-thickening, small-angle-neutron scattering measurements for micellar solution at rest
CPCl/NaSal, water	Sung et al. (2003)	rheological behavior depending on the surfactant concentration, identification of two critical concentrations that mark significant changes in viscosity behavior

Table 2.2: Literature studying different aspects of the rheological behavior of the selected surfactant solutions

Let us now briefly describe the experimental results and materials considered in the experimental works.

2.1 Colloidal suspensions

Colloidal suspension is a two-component system of the dispersed phase (the colloid) and the suspending medium. The dispersed particles are generally *too small to be easily observed by an optical microscope and they do not readily sediment in the liquid suspending phase* (Mewis and Wagner (2012)). Typical examples of the colloids are milk, ink or blood.

When sheared, colloidal suspensions can exhibit a wide variety of rheological phenomena, for example shear-thinning, shear-thickening, yield stress or jamming (see Brady and Bossis (1985)). In this section we present the particular behavior of one of the suspensions.

2.1.1 BiOCl/polyelectrolyte solution

In their work, Bertrand et al. (2002) present the experiment with bismuth oxychloride (BiOCl) in a very dilute polyelectrolyte solution. The performed measurements are stress-controlled with the plate-plate geometry[1] of the rheometer. The output experimental data have the form of viscosity-shear stress and viscosity-shear rate curves for different volume fractions. In relation with our work, the most remarkable curves are the ones that exhibit a slight backward bending. We have extracted[2] the viscosity - shear rate data for the volume fraction of 19% and we have plotted them into Figure 2.1b. The shear stress - shear rate curve plotted in Figure 2.1a is derived from the extracted data using the relation (1.17). This derivation requires that we assume that the viscosity treated in the scientific work is the apparent viscosity of the material.

2.2 Surfactant solutions

Lange (1999) adopts the definition of a surfactant as *a surface active amphiphile that aggregates in water or other solvent to form various microstructures such as micelles or bilayers*. The tendency of the amphiphilic molecules to self-assemble to form greater structures follows from their particular character. In fact they are characterized by containing both a solvophilic (typically hydrophilic) and a solvophobic (typically hydrophobic) part. Whereas the solvophilic part tends to react with the solvent, the solvophobic part is only poorly solvated (Lange (1999)).

[1] In the plate-plate geometry of the rheometer, the fluid fills the gap between two parallel and horizontally placed discs of which the upper one is rotating.

[2] All of the sets of data in this work have been extracted using the program g3data. The accuracy of the data is therefore given by the accuracy of this extracting method.

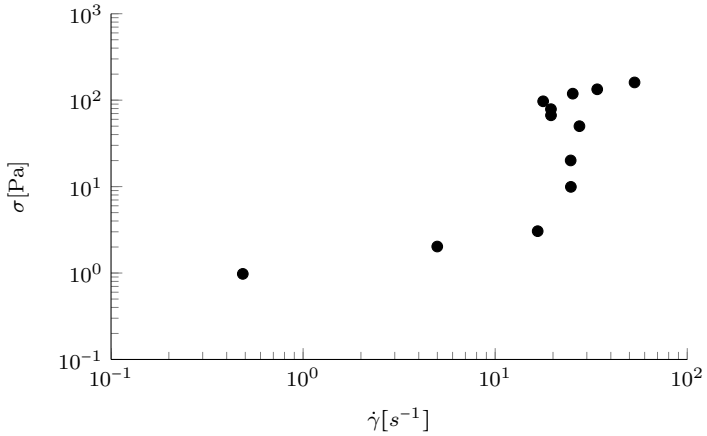

(a) Shear stress-shear rate dependence.

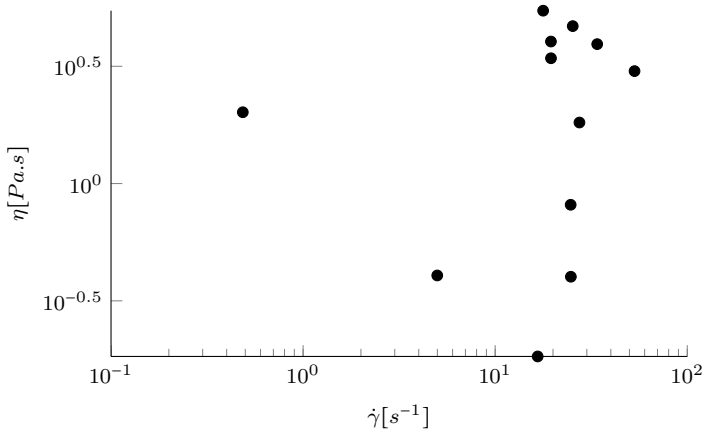

(b) Apparent viscosity-shear rate dependence.

Figure 2.1: Experimental data extracted from the work of Bertrand et al. (2002).

If hydrophilic parts of amphiphilic molecules carry a net charge, surfactant is characterized as ionic (cationic or anionic). Otherwise it can be nonionic or even zwitterionic. The zwitterionic surfactant is special for containing both, the positive and the negative charged groups attached to the same molecule.

2.2.1 Ionic surfactant TTAA

Experiments with the tris (2-hydroxyethyl) tallowalkyl ammonium acetate (abbreviated as TTAA) surfactant dissolved in water with an addition of salt (sodium salicylate) were performed by Boltenhagen et al. (1997b). This material was chosen because of its tendency to form very long wormlike micelles under the condition of low surfactant concentration. Moreover, as Boltenhagen and coworkers claim, *perhaps the most remarkable property of these systems is that they become much more viscous when sheared above a critical shear rate.*

The experiment was performed in a transparent glass Couette cell[3] attached to the

[3]Couette cell is an rheometrical device composed of two concentric cylinders of which the inner rotates. The fluid fills the gap between the cylinders.

rheometer. This experimental geometry allowed measurements under both, the constant shear stress and the constant shear rate. Both of the types of experimental data are extracted from the publication and plotted in Figure 2.2a. The derived apparent viscosity - shear rate curve is plotted in Figure 2.2b.

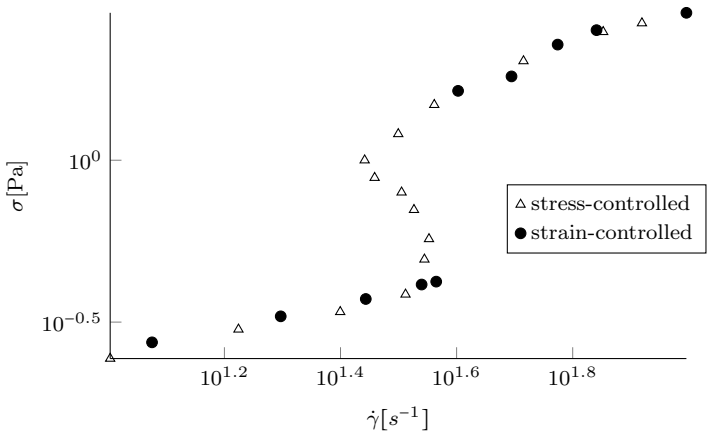

(a) Shear stress-shear rate dependence.

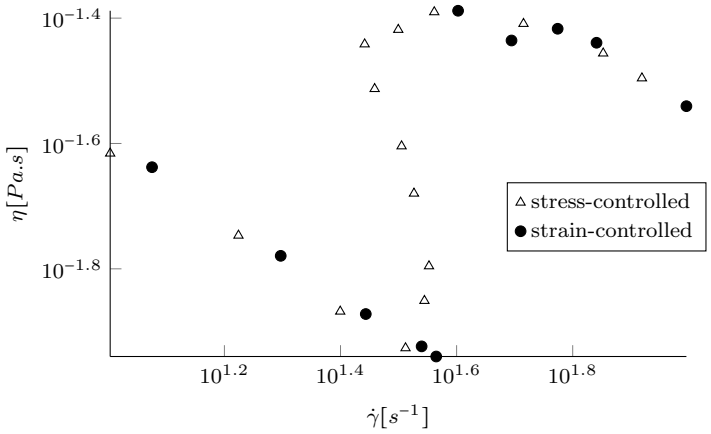

(b) Apparent viscosity-shear rate dependence.

Figure 2.2: Experimental data extracted from the work of Boltenhagen et al. (1997b).

Other experiments with the same TTAA/NaSal solution were performed by Hu and coworkers, see Hu et al. (1998a) and Hu et al. (1998b). The obtained stress - shear rate and apparent viscosity - shear rate curves are plotted respectively in Figure 2.3a, Figure 2.3b for the work of Hu et al. (1998a) and in Figure 2.4a, Figure 2.4b for Hu et al. (1998b).

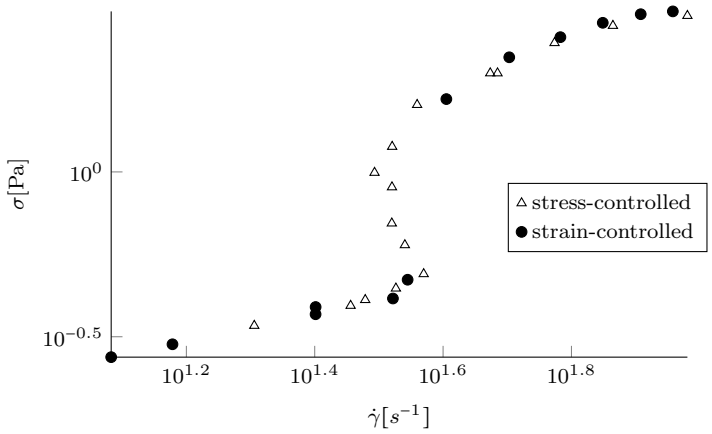

(a) Shear stress-shear rate dependence.

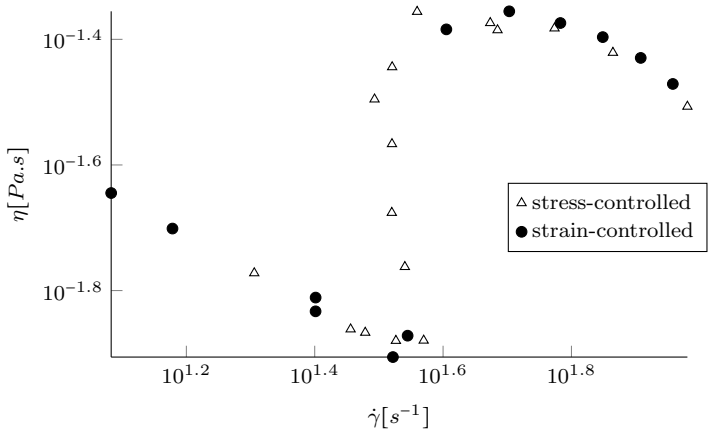

(b) Apparent viscosity-shear rate dependence.

Figure 2.3: Experimental data extracted from the work of Hu et al. (1998a).

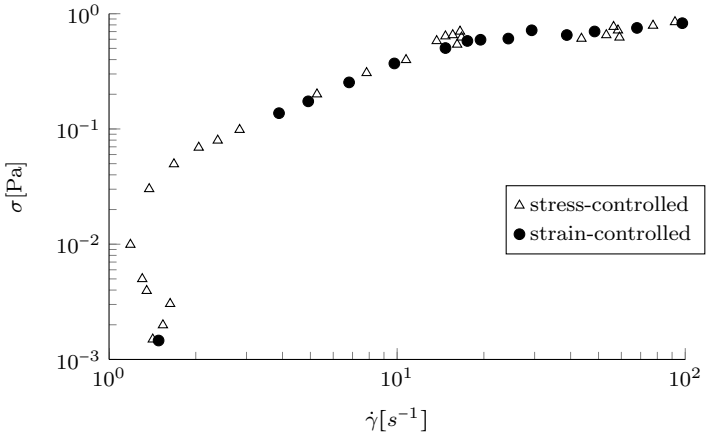

(a) Shear stress-shear rate dependence.

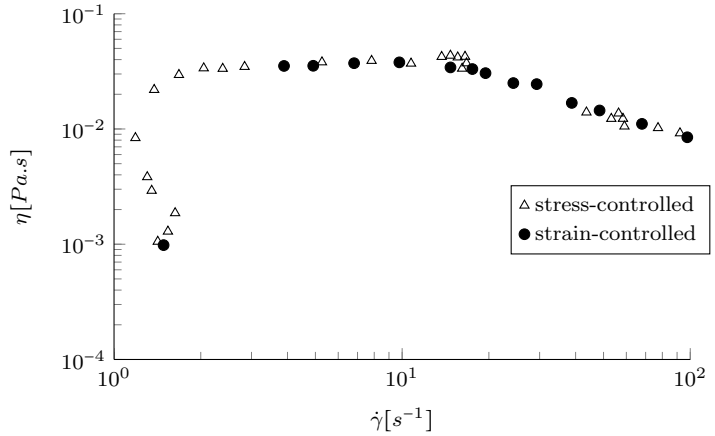

(b) Apparent viscosity-shear rate dependence.

Figure 2.4: Experimental data extracted from the work of Hu et al. (1998b).

Both of the experiments reveal the same behavior of the TTAA/NaSal solution under shear as the first experiment performed by Boltenhagen et al. (1997b) does. In addition, works contain a very detailed visualization of the structural changes of the system in time. The included scattering images thus make a complete view on the process of the shear-induced structures creation by the system.

2.2.2 Cationic surfactant CTAT

Measurements performed by Macias et al. (2001) with the solution of cethyltrimethylammonium tosylate (abbreviated CTAT) in water show similar results to the results obtained for a TTAA/NaSal solution. In their experiment, Macias and coworkers investigate the behavior of the 25wt%[4] solution that is subjected to shear in two types of Couette cell geometries. Experimental data from both the shear rate-controlled and the shear stress-controlled measurements are plotted in Figure 2.5a. The derived apparent viscosity-shear rate curves are plotted in Figure 2.5b.

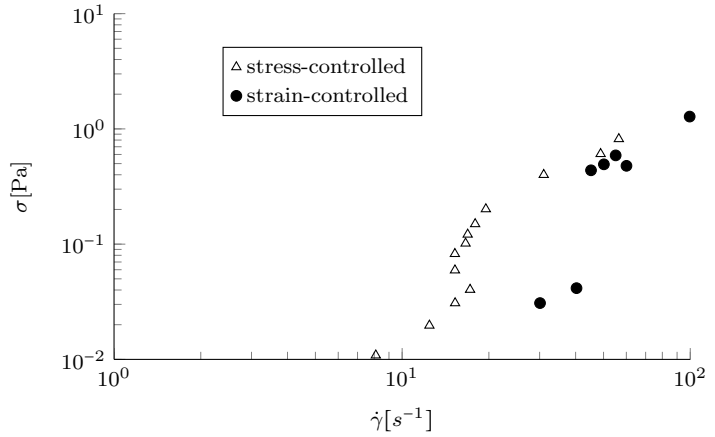

(a) Shear stress-shear rate dependence.

[4]wt% denotes the weight percent.

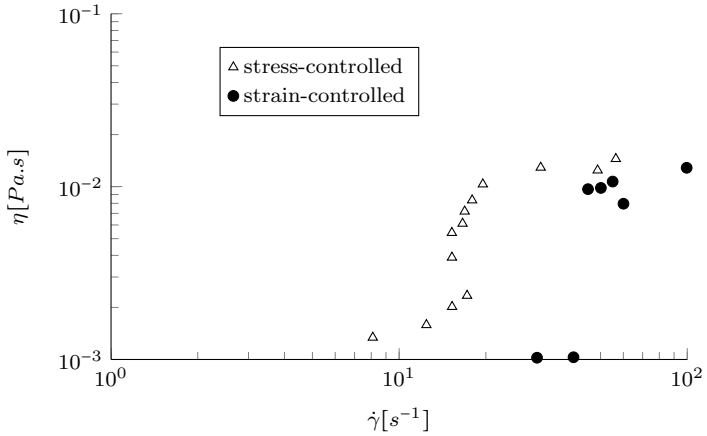

(b) Apparent viscosity-shear rate dependence.

Figure 2.5: Experimental data extracted from the work of Macias et al. (2001).

2.2.3 Zwitterionic surfactant TDPS, anionic surfactant SDS and brine

Lopez-Diaz et al. (2010) present in their work the experimental study of the mixture of the N-tetradecyl-N,N-dimethyl-3-ammonio-1-propanesulfonate (abbreviated TDSP) and sodium dodecyl sulfate (abbreviated as SDS) in the solution with water. The measurements of the shear stress and of the apparent viscosity as the function of the shear rate were performed for various values of the parameters such as zwitterionic surfactant concentration, temperature and two surfactant ratio. Their experimental results show that the mixture of TDPS and SDS is a surfactant that exhibits an S-shaped flow curve in the stress-controlled type of measurement under suitable conditions. Experimental data from stress-controlled and shear rate-controlled measurements are plotted in Figure 2.6a. The derived apparent viscosity-shear shear rate curve is plotted in Figure 2.6b.

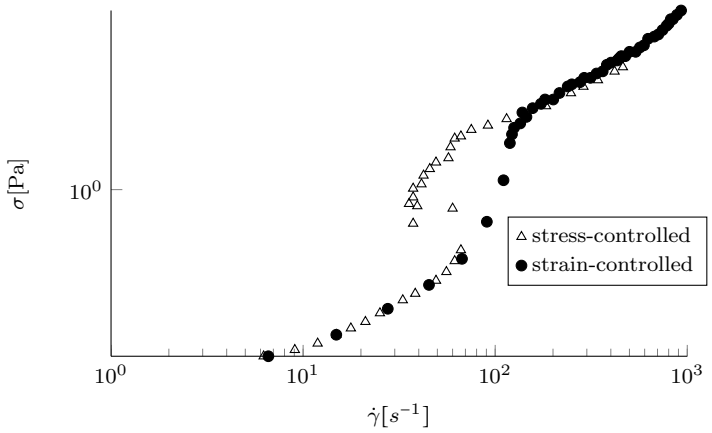

(a) Shear stress-shear rate dependence.

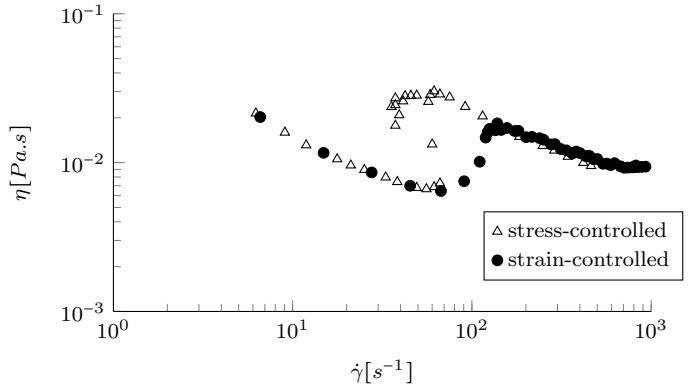

(b) Apparent viscosity-shear rate dependence.

Figure 2.6: Experimental data extracted from the work of Lopez-Diaz et al. (2010).

2.2.4 Anionic surfactant SDS, dodecane, pentanol and water

In their work, Roux et al. (1993) study the system composed of the anionic surfactant sodium dodecyl sulfate (SDS), dodecane and pentanol in aqueous solution by performing stress-controlled measurements. The system forms a lyotropic lamellar phase[5] that behaves in a specific manner when subjected to shear in solution. The shear stress-shear rate dependence thus can take an untypical shape; the one that was experimentally obtained contain a backward bending part. Experimental data are plotted in Figure2.7a and the derived apparent viscosity-shear rate curve is plotted in Figure 2.7b. The same experiment was later performed by Wilkins and Olmsted (2006) and led to the shear stress-shear rate experimental data of stress-controlled measurements for different time intervals of the stress-sweep (see Wilkins and Olmsted (2006), Figure 4). The data corresponding to the steady state conditions are plotted in Figure 2.8a. The derived viscosity data are plotted in Figure 2.8b.

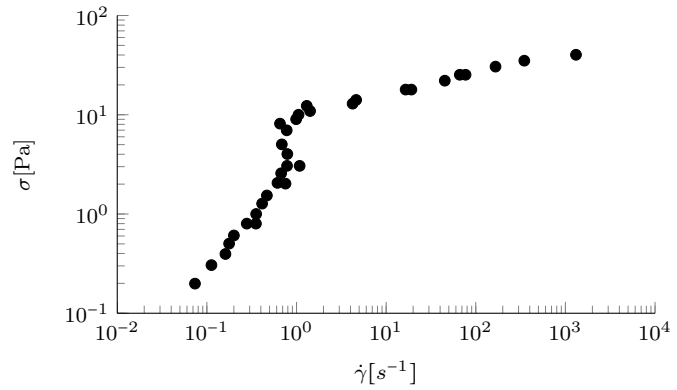

(a) Shear stress-shear rate dependence.

[5]At high concentrations, surfactant molecules arrange in the way that they form bilayers separated by layers of the solvent. This ordered structure is called *lamellar* and is characteristic for liquid crystals. The notion *lyotropic* refers to the induction of the ordered structure by effects of the addition of a solvent; see Section 3.1.2

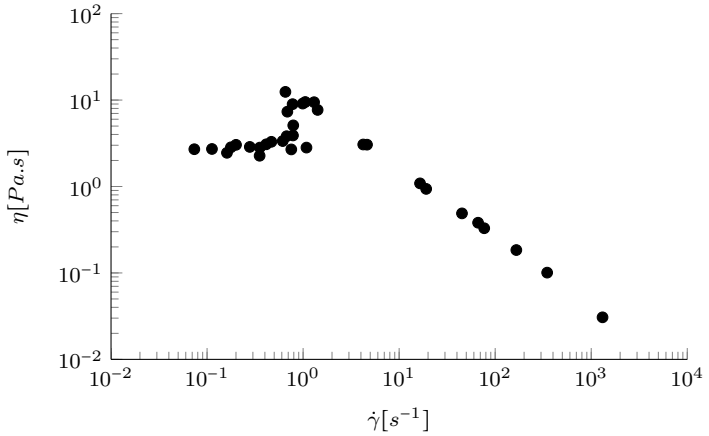

(b) Apparent viscosity-shear rate dependence.

Figure 2.7: Experimental data extracted from the work of Roux et al. (1993).

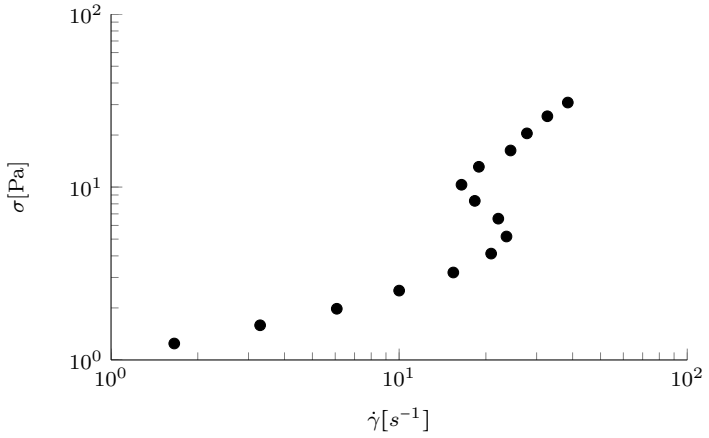

(a) Shear stress-shear rate dependence.

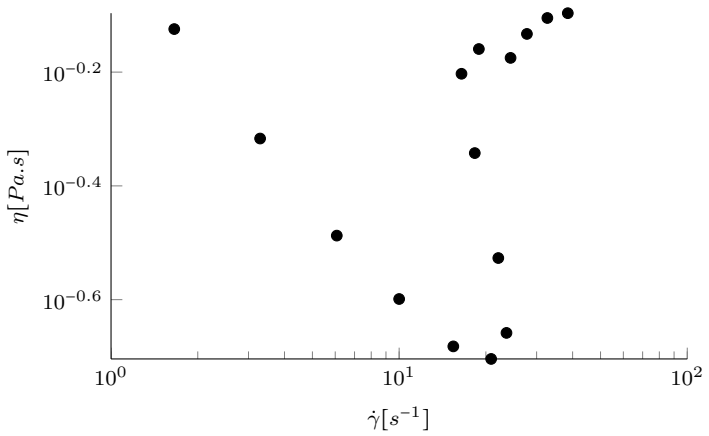

(b) Apparent viscosity-shear rate dependence.

Figure 2.8: Experimental data extracted from the work of Wilkins and Olmsted (2006).

3. Microscopic theories

In this section we will present some existing microscopic theories that explain the shear-thickening, the shear-thinning and the shear banding behavior of colloidal and surfactant solutions. In this way we want to suggest to the reader the idea of microscopic processes that occur in a non-Newtonian fluid. This would help him to understand the structural transitions of a fluid whose behavior is characterized by an S-shaped shear stress-shear rate dependence.

3.1 Concepts explaining the shear-thickening and shear-thinning phenomena

3.1.1 Colloidal suspensions

Hydrodynamic clustering

Brady and Bossis (1985) explain the increase in viscosity of a colloidal suspension by formation and growth of hydrodynamic clusters. The clusters are compact groupings of colloid particles that act as a single particle due to short-range lubrication forces. Brady and Bossis (1985) claim that *a force exerted on one particle at the end of a cluster is 'transmitted', almost as if the particles were in actual contact, to the other end of the cluster via the lubrication forces and the connectivity of the structure.* The theory of hydrodynamic clustering was approved by experiments performed by Cheng et al. (2011). Based on the experimental data, Cheng et al. (2011) make an illustrating visualization of the clustered suspension represented in Fig. 3.1.

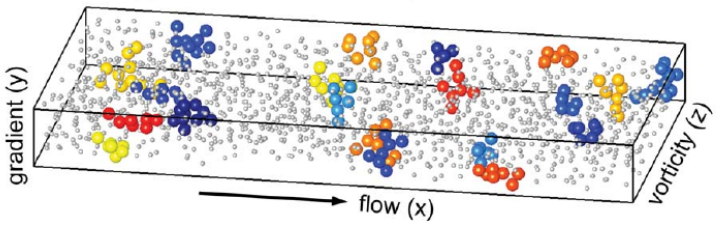

Figure 3.1: *Instantaneous real-space configuration of hydroclusters* (Cheng et al. (2011)). Identified singular hydroclusters are represented with colours; other particles are white-grey. The size of boundary box is 31,2 by 15,4 by 3,1 μm.

Order-to-disorder transition

In his work, Hoffman (1972) studies the shear-thickening behavior of monodisperse suspensions. According to the light diffraction observations, he claims that the shear-thickening is caused by an order-to-disorder transition of the fluid structure. At low

shear rates, suspending particles are organized into layers that are for most of viscometric flows *parallel to surfaces of constant shear*. At a critical shear rate, the layered structure is damaged due to the flow instability. Particles are then redistributed, forming a less ordered structure which causes a rise in viscosity. Hoffman (1972) reports that for suspensions of monodisperse particles that are highly concentrated, the rise in viscosity at a critical shear rate is discontinuous. Hoffman (1974) develops a mathematical model to predict the occurrence of such a behavior.

Various later performed experiments have not approved the validity of the suggested order-to-disorder theory. The small angle neutron scattering observations made for example by Bender and Wagner (1996), Fagan and Zukoski (1997) and Chow and Zukoski (1995) have shown that the shear thickening of the studied suspensions is not related to the layered-to-unlayered transition. To explain the shear-thickening process in these experiments, other theories are proposed of which the principal is the cluster formation, see Section 3.1.1. Hoffman (1998) finds the suggestions that refute the presence of the order-to-disorder transition in the studied fluids doubtful. In particular, he finds the small angle neutron scattering method inappropriate to prove the absence of the transition. Indeed the method requires ordered structure within layers in order to show accurately the changes in the structure. The ordering of particles within a layer is however not involved in the order-to-disorder transition model. Hoffman (1998) underlines this fact and reformulates his theory in appropriate manner: *Before shear-thickening occurs, particles move in layers, but they do not have to be rigorously ordered in these layers, and the layers can have a thickness ranging from one particle diameter to some multiple of the average particle diameter. Then, at the onset of shear-thickening, a hydrodynamic instability acts to drive particles out of these layers. When this happens, the particles interact through clustering and/or through physical contact.*

Jamming phenomenon

Upon shearing, a colloidal suspension can undergo a jamming transition that leads to an amorphous solid state developing the yield stress. Yield stress is the phenomenon that has been moreover measured in some shear-thickening fluids. The exact relation between the yield stress and the shear-thickening or between the shear-thickening and the jamming has not however yet been clearly established. Let us see some theories and observations suggested in this context.

To examine similarities between the shear-thickening and the jamming, Brown and Jaeger (2009) have performed experiments with two colloidal suspensions, cornstarch in water and glass spheres in mineral oil. On the base of the measured shear stress-shear rate data for various packing fractions, they have created the so-called dynamic jamming phase diagram. The diagram *delineates shear-thinning, shear-thickening and jammed regions in a parameter space given by the applied stress and the packing fraction.*

Its role is therefore to give us the idea of the occuring phenomena if the stress and the packing fraction are fixed. Brown and Jaeger (2009) conclude that the relation between the shear-thickening and the jamming involves the limiting process, precisely that *the discontinuous shear-thickening limit corresponds to a jammed state* (for the view of the diagram and its detailed description, see Brown and Jaeger (2009)).

The relation between the shear thickening and the jamming of colloidal substances was examined also by Bertrand et al. (2002). They present the performed experiments with the suspension of bismuth oxychloride. In their work they show that *shearing a suspension may lead to either thickening or permanent jamming, depending on the volume fraction of the suspension.* At high volume fractions (22.5% - 31%) it is the phenomenon of the shear-induced jamming transition that occurs. This state is however metastable in the sense that it can come back to the original liquid phase by small perturbations, for example by putting a drop of liquid phase into contact with it. Otherwise, Bertrand et al. (2002) have noticed that the jammed state is stable kinetically. It persists if no shear rate is applied. They claim that this property makes the difference between a jammed and a shear-thickened state that is, in contrast, kinetically *purely transient*. They suggest finally that the two phenomena may be the consequences of a common dynamical structural transition.

Let us now make a reasoning about the nature of the jammed state. Some models are presented by Cates et al. (1998) who suggest that a jammed colloid is formed by an assembly of force chains. These chains are understood as *linear strings of rigid particles in point contact*. In order to make approach about the stability, Cates et al. (1998) introduce the concept of the class of materials named 'fragile matter' that includes the jammed colloid. The characteristic property of the included materials is the mechanical instability in some directions. Liu and Nagel (see Liu and Nagel (1998)) explain it as follows: *Although it can support a large applied load in the same direction as the original jamming forces, the chain will fall apart if even an infinitesimal force is applied in a different direction.* An illustration of a jammed colloid with force chains is shown in Figure 3.2.

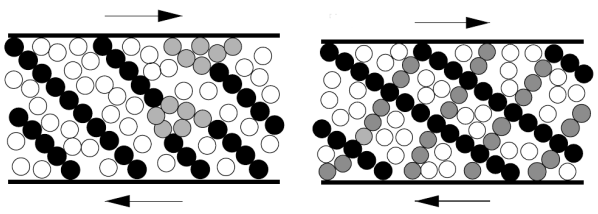

Figure 3.2: Force chain model of a jammed colloid. Left: a jammed state, right: idealized network of force chains; force chains are black, other *force-bearing* particles are grey and spectator particles are white (Cates et al. (1998)).

A semi-empirical theory

Several models were developed on the base of the semi-empirical theory named *Soft glassy rheology* (SGR). The theory was designed by Sollich (see Sollich et al. (1997) in order to describe the rheology of soft materials such as foams, dense emulsions, pastes and slurries. This concept basically unifies the soft materials and it has been developed as the consequence of observed similarities of their anomalous rheological behavior under specific conditions. The theory serves as the base of several models of shear-thickening and jamming developed for example in Head et al. (2001).

3.1.2 Surfactant solutions

In aqueous solution, surfactants exhibit a behavior particularly interesting from the rheological point of view. If their concentration is greater than or equal to the critical value (the so-called critical micelles concentration - CMC), their molecules have tendency to self-assemble reversibly into larger objects (Figure 3.3). The type of the created aggregates depends on the concentration of the surfactant, of eventually added salts and on the temperature. For low surfactant concentrations, molecules self-assemble into spherical micelles (Figure 3.4a). Increasing the concentration, they tend to create cylindrical structures (Figure 3.4b) that form more complexes wormlike structures by further overlapping and entangling. At still higher concentrations, they assemble to form mesophases with nematic, hexagonal or lamellar ordering (Figure 3.4c). Transitions between particular types of molecular aggregates are possible also by varying temperature and salts concentration (Cates and Fielding (2007)).

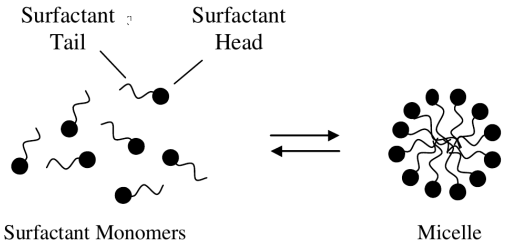

Figure 3.3: Micelle formation in a low-concentrated surfactant solution. Surfactant head represents the solvophilic part and the tail is the solvophobic part of an amphiphilic molecule; Rangel-Yagui et al. (2004).

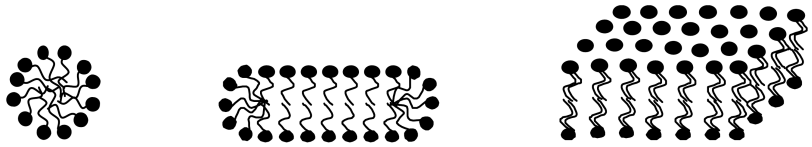

(a) (b) (c)

Figure 3.4: Various existing self-assembled aggregates in surfactant solution. Spherical micelles (a); cylindrical micelles (b); lamellar ordering (c); Rangel-Yagui et al. (2004).

Solutions of wormlike micelles

Wormlike micelles are elongated aggregates of surfactant molecules formed by self-assembling in concentrated solutions. In many physical aspects, they resemble polymer chains but in the aspect of the behavior in solution under shear, they do not. While wormlike micelles are dynamic in their behavior so that their structure is capable of breaking and of the reversible recreation, polymers are less flexible. Intense shearing of polymers may cause a permanent reduction of the chains (see Cates and Fielding (2007) and Cates and Candau (1990)).

Experiments show that solutions of wormlike micelles can exhibit either shear-thinning or shear-thickening behavior. While the shear-thinning behavior is generally explained as the process of alignment of originally entangled micelles (see Förster et al. (2005)), the shear-thickening behavior remains poorly understood.

The shear-thickening phenomenon was experimentally studied by Boltenhagen et al. (1997a), Hu et al. (1998a), Hu et al. (1998b) and Liu and Pine (1996) on samples of very dilute surfactant solutions. Viscosity measurements and visualizations by light scattering have provided evidences for the existence of the critical shear rate that marks the change in the solution behavior. For shear rates below this value, the solution exhibits the shear-thinning behavior. For shear rates above the critical value, the behavior is time dependent. First, there is a period of time (named 'induction time') characterized by a relatively constant viscosity. The duration of this time period is dependent on the concentration of the solution and on the applied shear rate, see Liu and Pine (1996). Then the solution exhibits the shear thickening with a sharp rise in viscosity. Scattering images and simultaneous measurements performed by Boltenhagen et al. (1997a) show that the shear-thickening correlates with the growth of a highly scattering region, named shear-induced structures (SIS) or phases (SIP) (see also Boltenhagen et al. (1997b), Hu et al. (1998a)). The formation of this phase is therefore supposed to be the origin of the shear-thickening. To determine the nature of the formed phase, several scattering experiments have been performed. Scattering images obtained by Boltenhagen et al. (1997a) show that the formed SIS is a highly entangled system that is more viscous than the unsheared fluid. SIS appears to grow as finger-like structures under shear and then progressively fills the entire gap where the initial solution was

placed, that is analogical to the observations from experiments performed by Liu and Pine (1996).

Other types of experiments that aim to explain the shear-thickening process in solutions of wormlike micelles have been performed by Keller et al. (1998). Keller et al. (1998) have used two surfactant solutions (TTAA/NaSal and CTAB/NaSal) that they subjected to shear and they observed progressively their structural transitions by the freeze-fracture electron microscopy (FFEM). Rheological measurements and visualizations show that new structures (of the order of μm) are formed and that they are much larger than the individual micelles (of the order of nm). Moreover they appear consistent with the light scattering results, see Liu and Pine (1996) and Boltenhagen et al. (1997b). Additionally, the experiments show that the structures have the tendency to assemble and to connect in order to form larger superstructures with the size of hundreds of microns. The new created structures have a spongelike texture and they are richer in surfactant than the surrounding micellar solution. Keller et al. (1998) conclude that this phase is likely to be the origin of the shear-thickening in micellar solutions.

Despite the scattering and the freeze-fracture microscopy visualizations, the nature of the shear-thickened state remains unclear. Several models have been suggested in order to create another view to the process.

Wang (1992) presents a model of the shear-thickening for solutions of wormlike micelles based on the idea of the creation of a reversible network system with temporary cross-links, see Figure 3.5. The network is for simplicity assumed nonentangled; it is formed merely by bonds among functional groups at micellar ends. Wang introduces three types of micellar chains in the system where a network is formed: the ones with both ends incorporated in the network, the other ones with only one end bounded and the last ones: free unbounded chains. On the base of these ideas, the model explains the shear-thickening of a system as due to more chains participating in the networking. Hence shearing of the system leads to incorporation of free chains into the network.

The shear-thickening process can however be viewed in some other ways. Cates and Candau (2001) assume that the solution includes the structures in the form of large rings that link and break, and control in this way the shear-thickening process. Cates and Turner (1990) propose the process of the growth of micelles as the origin of the shear-thickening. Bruinsma et al. (1992) make analogies between the behavior of wormlike micellar solutions and of colloidal suspensions and explain the shear-thickening of micellar solutions on the base of the colloidal coagulation (process of particle aggregation induced by shear flow discovered by Paine (1912). Barentin and Liu (2001) suggest that the shear-thickened state consists of a network bundle.

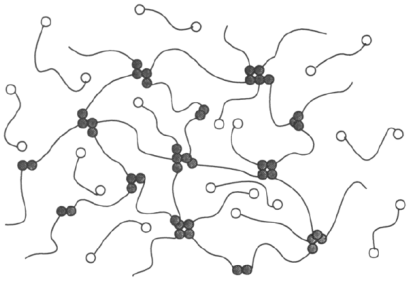

Figure 3.5: Micellar network; three types of micellar chains introduced by Wang (1992): chains with both ends bounded, chains with one end bounded and unbounded chains. Bonds are represented as full circles and unbounded ends as white circles. Figure extracted from the work of Wang (1992).

Surfactant solutions with lamellar ordering of molecules

At high concentrations (surfactant ratio > 30%), surfactants in solution act as lyotropic liquid crystals. Having the character of a liquid crystal means that *the solution possesses static and dynamic properties associated to both the crystalline organization (long-range translational order, elasticity) and the liquid properties (viscosity, concentration fluctuations...)*, see Diat et al. (1993). Being lyotropic signifies that its ordered structure is induced by addition of a solvent. Under shear, the solution exhibits significant structural changes. The characteristic ordered lamellar phase is rearranged and the process results therefore in an increase of the viscosity.

Lyotropic lamellar phases and their rheology were studied by Diat et al. (1993) and Roux et al. (1993). The system investigated in the experiments is a mixture of the anionic surfactant SDS (sodium dodecyl-sulphate), pentanol, water and dodecane. Fixing various parameters of the solution, the distances between the individual lamellae were stabilized on values from the interval from 40 Å to 400 Å.

Shear rate-controlled experiment with the investigated solution in a Couette cell geometry has been performed by Diat et al. (1993). The results show evidences of three existing flow regions associated with the orientation of the lamellar phase. At low and high shear rates, the orientation corresponds to the layers with the normal that points along the radial velocity gradient direction. The difference between these two regions consists in the internal orientation within a layer (in the vorticity-flow plane). At intermediate region of shear rates, visualizations show the existence of a completely isotropic orientation. The layers are *wrapped around a spherical core forming large* multilayer *objects* (the onionlike structures). The structures are generally larger than the distance separating the layers in a non-sheared solution. Their size is however highly dependent on the intensity of the shearing.

Roux et al. (1993) have studied the nature of the transitions between the individual regimes and they have performed the stress-controlled measurements with the

investigated solution. The obtained data of the shear stress-shear rate dependence are included in our review of the curves with the backward bending part, see Figure 2.7a. Analogical experiments were also performed by Wilkins and Olmsted (2006). Wilkins and Olmsted (2006) have studied the rheological behavior of the solution by putting it into analogy with the results from the rheological experiments with wormlike micelles. They underline the observed similarity in the measured flow curves: the shear stress exhibits a discontinuity at a given shear rate. Wilkins and Olmsted (2006) suggest that this discontinuity in the behavior of the studied lyotropic lamellar solution is associated with the existence of *bands of lamellae and onionlike structures stacked in the vorticity direction.* The bands have in this geometry the same shear rate but different shear stresses (see Section 3.2). Wilkins and Olmsted (2006) conclude suggesting that the lamellar-to-onion transition for the mixture of SDS, pentanol, water and dodecane corresponds to the vorticity banding. Currently, they are working on experimental evidences for the hypothesis.

(a) (b)

Figure 3.6: Schema of lamellar (a) and onionlike (b) structures formed by surfactant molecules in solution;Ganguli et al. (2010).

3.2 Shear banding

Under specific conditions of shearing materials as polymers, liquid crystals, colloidal suspensions and especially surfactant solutions, two or more solution bands can appear, separated by a stable interface. This occurring phenomenon is called the shear banding and arises for a specific interval of the shear rates or shear stresses. According to the direction of the normal to the interface between the bands, we distinguish gradient banding (normal directed in the velocity gradient direction) and vorticity banding (normal directed in the vorticity direction) that is illustrated in Figure 3.7.

The condition of momentum balance in the steady state implies that in a planar shear flow the shear rate and the shear stress must be uniform respectively in the vorticity and the gradient direction. This in turn implies that in the vorticity banding, bands have the same shear rate and they differ by the shear stress. Inversely, bands formed in the gradient banding have the same shear stress but different shear rates, see Olmsted (2008).

(a) (b)

Figure 3.7: Gradient banding (a) and vorticity banding (b) in a plate-plate geometry. The numbers I and II refer to the particular bands and the arrows indicate the direction of the shearing; Goveas and Olmsted (2001).

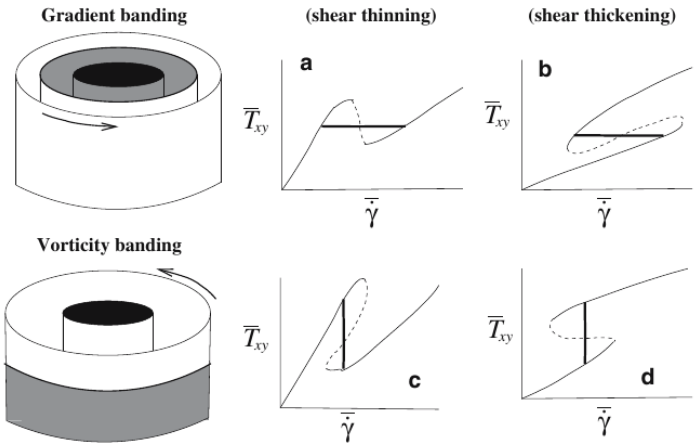

Figure 3.8: Constitutive curves that are candidates for exhibiting the shear-banding behavior (T_{xy} denotes the shear stress). Stable constitutive curves are represented by thin lines. Dashed lines are unstable flows; a fluid must separate into stable bands in this region. The stable part corresponding to a shear-banded state is represented by thick lines. The overbars designate the average value imposed by the rheometer; Olmsted (2008).

Shear stress-shear rate curves we are focusing on in this work have the shape of the character S. According to the categorization of the curves made by Wilkins and Olmsted (2006) shown in Figure 3.8, the S-shaped type corresponds specifically to the vorticity banding phenomenon. Boltenhagen et al. (1997b) reveal experimentally the existence of a counterexample. The stress-controlled experiments with the surfactant solution of the tris (2-hydroxyethyl) tallowalkyl ammonium acetate (TTAA) reveal that the solution with the S-shape curve exhibit the phenomena of the shear-thickening and the gradient banding (see Figure 2.2a in Section 2)

The problematic part of an S-shaped curve is the backward bending region (the loop) that is not stable. The behavior of the solution is in this region highly dependent on the character of the performed measurements. Two types of measurements are performed to see these differences: the rate-controlled and the stress-controlled ones.

The first type indicates that the shear rate is imposed to the system and the shear stress is optional to it. Measurements with wormlike micellar solutions (see Boltenhagen et al. (1997b))show that if we impose the critical value of the shear rate in the non-monotonic regime, the system pass from the homogeneous flow of a lower viscosity to the homogeneous flow of a higher viscosity with no stable state of coexistence. This process of shearing the system is thus marked by a discontinuous increase in viscosity. Consequently, it *leaves a range of stresses that is unattainable* by the system (see Cates and Fielding (2007)).

In contrary, the stress-controlled measurements with wormlike micellar solutions show another evolution of the system rheology (see Boltenhagen et al. (1997b)). When the solution is sheared in the domain of the backward bending region, the phenomenon of the gradient banding occurs, giving birth to two coexisting phases. This process is therefore marked by no discontinuity in the viscosity. Imposing a specific value of the shear stress that is included in the bending region, a shear-induced more viscous phase begins to appear in the direction of the velocity gradient. Hence the induced phase coexists with the original one with a stable interface between them. Increasing the stress, the ratio of the shear-induced phase in the system increases. Reaching a specific stress value, the system is entirely formed by the high-viscous shear-induced phase.

The idea of the shear banding is in detail developed in Goveas and Olmsted (2001), Wilkins and Olmsted (2006), Olmsted (2008) and Cates and Fielding (2007).

———

4. Interpolation of experimental data

In Section 2 we presented several experimental data of the dependence of the shear stress σ on the shear rate $\dot{\gamma}$ in a simple shear flow. The data have the form of backward bending curves and cannot thus be described with a classical type of one-dimensional constitutive relation $\sigma = f(\dot{\gamma})$ where f is a scalar function. In this part of our work, we will present several implicit type relations that can be used to fit the data of this type and we will moreover show some examples of their application.

4.1 One-dimensional constitutive relations

In order to fit experimental data with a backward bending part, we investigate the one-dimensional constitutive relation in the form $\dot{\gamma} = g(\sigma)$ where g is a scalar function. In particular, we will be interested in the following relations

$$\dot{\gamma} = \mathrm{e}^{-a\sigma}\left(a_1\sigma + a_2\right) + \left(1 - \mathrm{e}^{-b\sigma}\right)\left(b_1\sigma + b_2\right), \tag{4.1a}$$

$$\dot{\gamma} = \frac{p_1\sigma^3 + p_2\sigma^2 + p_3\sigma + p_4}{\sigma^2 + q_1\sigma + q_2}, \tag{4.1b}$$

$$\dot{\gamma} = \left(\alpha\left(1 + \beta\sigma^2\right)^n + \gamma\right)\sigma + \eta. \tag{4.1c}$$

The relations (4.1a) and (4.1b) have been selected according to the analysis of the experimental data that they will fit. As can be noticed from the graphs of the shear stress - shear rate dependence (see for example Figure 2.2a), the solution behaves as a Newtonian fluid in a range of small applied shear stresses. This fact apparently induces a restriction on the constitutive relation in the region of small stresses; it must be linear in the limit $\sigma \to 0$. In the range of large stresses, the situation is the same; the linear response of the material on the stress implies the linear character of the relation in the limit $\sigma \to \infty$. For medium stresses, the relation must have the appropriate number of degrees of freedom to suit the required shape. The relation (4.1c) is taken as a one-dimensional alternative of the expression proposed by Málek et al. (2010) that states $\mathbb{D} = \alpha(1 + \beta|\mathbb{T}_\delta|^2)^n\mathbb{T}_\delta$, with the addition of the yield stress η.

4.2 Interpolation of experimental data

From the list of experimental data presented in Section 2, we have chosen the ones plotted in Figure 2.2a and in Figure 2.3a (we do not show the errorbars that are present

in the original publication). We have fitted them with the relations (4.1a), (4.1b) and (4.1c) and we have reported the fits in this section. All of the interpolations have been done by the method of weighted least squares as it is implemented in Curve Fitting Toolbox™ in MATLAB. The fitted values of coefficients and the corresponding conficence bounds shown in tables in this section are the values that have been directly extracted from MATLAB, without rounding or other modifications.

curve A	$\dot{\gamma} = \mathrm{e}^{-a\sigma}\left(a_1\sigma + a_2\right) + \left(1 - \mathrm{e}^{-b\sigma}\right)\left(b_1\sigma + b_2\right)$
curve B	$\dot{\gamma} = \frac{p_1\sigma^3 + p_2\sigma^2 + p_3\sigma + p_4}{\sigma^2 + q_1\sigma + q_2}$
curve C	$\dot{\gamma} = \left(\alpha\left(1 + \beta\sigma^2\right)^n + \gamma\right)\sigma + \eta$

Table 4.1: Notation of interpolating curves.

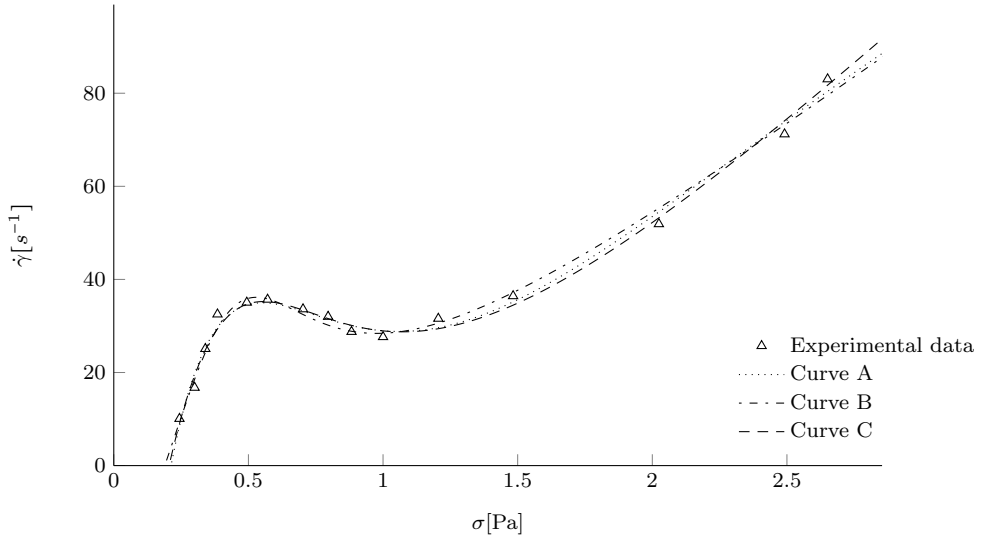

Figure 4.1: Fit of stress-controlled experimental data; Boltenhagen et al. (1997b).

Curve A

Coefficient	Fitted value	Unit	95% confidence bounds
a	0.005156	Pa^{-1}	(-0.06523, 0.07554)
a_1	817	$s^{-1}Pa^{-1}$	(101.2, 1533)
a_2	-128.8	s^{-1}	(-221.1, -36.52)
b	3.135	Pa^{-1}	(0.702, 5.568)
b_1	-753.4	$s^{-1}Pa^{-1}$	(-1226, -280.9)
b_2	67.99	s^{-1}	(-328.7, 464.7)

Curve B

Coefficient	Fitted value	Unit	95% confidence bounds
p_1	43.12	$Pa^{-1}s^{-1}$	(31.16, 55.07)
p_2	-71.88	s^{-1}	(-107.2, -36.59)
p_3	52.01	Pas^{-1}	(15.72, 88.29)
p_4	-7.563	Pa^2s^{-1}	(-13.98, -1.146)
q_1	-0.7231	Pa	(-1.011, -0.4348)
q_2	0.2746	Pa^2	(0.1789, 0.3703)

Curve C

Coefficient	Fitted value	Unit	95% confidence bounds
α	333	$Pa^{-1}s^{-1}$	(72.45, 593.6)
β	2.299	Pa^{-2}	(-1.124, 5.722)
γ	54.39	$Pa^{-1}s^{-1}$	(42.78, 66.01)
η	-69.67	s^{-1}	(-118.9, -20.49)
n	-1.691		(-3.238, -0.1446)

Table 4.2: Fitted values of coefficients in relations (4.1a), (4.1b) and (4.1c) for the stress-controlled data Boltenhagen et al. (1997b).

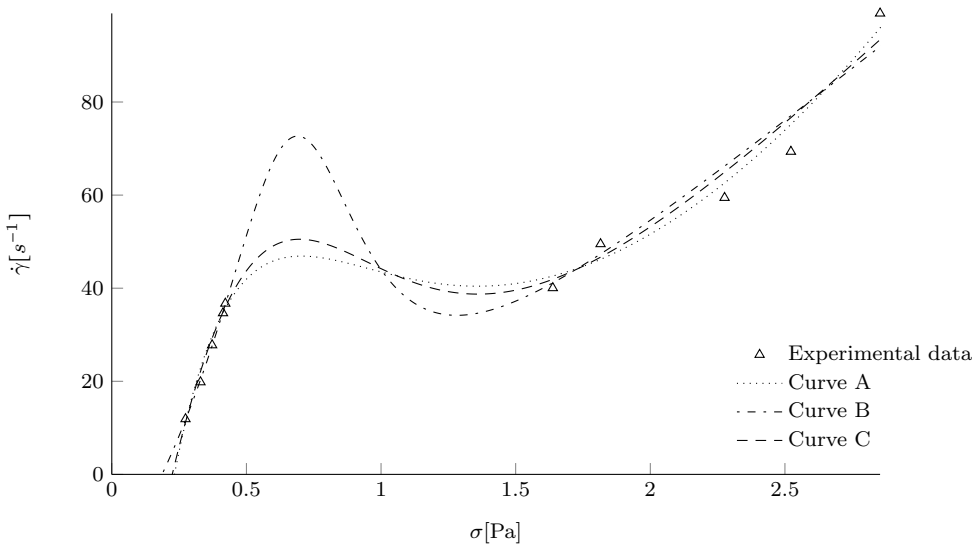

Figure 4.2: Fit of rate-controlled experimental data; Boltenhagen et al. (1997b).

Curve A

Coefficient	Fitted value	Unit	95% confidence bounds
a	0.008176	Pa^{-1}	(-0.05324, 0.06959)
a_1	917.7	$s^{-1}Pa^{-1}$	(232.6, 1603)
a_2	-143.9	s^{-1}	(-240.8, -46.87)
b	3.262	Pa^{-1}	(1.011, 5.512)
b_1	-843.3	$s^{-1}Pa^{-1}$	(-1297, -389.6)
b_2	75.05	s^{-1}	(-306.8, 456.9)

Curve B

Coefficient	Fitted value	Unit	95% confidence bounds
p_1	43.01	$Pa^{-1}s^{-1}$	(30.93, 55.08)
p_2	-70.46	s^{-1}	(-104.7, -36.23)
p_3	51.05	Pas^{-1}	(16.25, 85.86)
p_4	-7.541	Pa^2s^{-1}	(-13.78, -1.298)
q_1	-0.6909	Pa	(-0.9717, -0.41)
q_2	0.2549	Pa^2	(0.1707, 0.339)

Curve C

Coefficient	Fitted value	Unit	95% confidence bounds
α	390.2	$Pa^{-1}s^{-1}$	(60.21, 720.3)
β	2.982	Pa^{-2}	(-1.209, 7.173)
γ	56.96	$Pa^{-1}s^{-1}$	(44.2, 69.73)
η	-80.08	s^{-1}	(-140.5, -19.7)
n	-1.459		(-2.639, -0.2776)

Table 4.3: Fitted values of coefficients in relations (4.1a), (4.1b) and (4.1c) for the rate-controlled data Boltenhagen et al. (1997b).

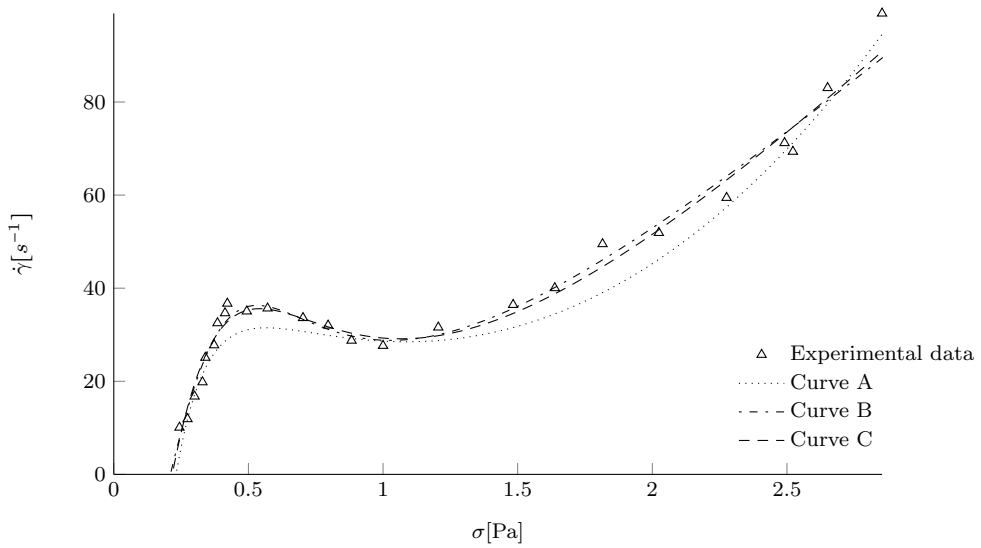

Figure 4.3: Fit of both the stress-controlled and the rate-controlled experimental data; Boltenhagen et al. (1997b).

Curve A

Coefficient	Fitted value	Unit	95% confidence bounds
a	-0.03681	Pa^{-1}	(-0.6141, 0.5404)
a_1	423.5	$s^{-1}Pa^{-1}$	(-2803, 3650)
a_2	-126.7	s^{-1}	(-719.6, 466.1)
b	2.787	Pa^{-1}	(-17.68, 23.25)
b_1	-444.7	$s^{-1}Pa^{-1}$	(-2932, 2043)
b_2	163	s^{-1}	(-1659, 1985)

Curve B

Coefficient	Fitted value	Unit	95% confidence bounds
p_1	46.31	$Pa^{-1}s^{-1}$	(3.666, 88.95)
p_2	-103.5	s^{-1}	(-347.7, 140.8)
p_3	78.15	Pas^{-1}	(-208.8, 365.1)
p_4	-11.28	Pa^2s^{-1}	(-58.66, 36.09)
q_1	-1.359	Pa	(-5.171, 2.453)
q_2	0.58	Pa^2	(-1.754, 2.914)

Curve C

Coefficient	Fitted value	Unit	95% confidence bounds
α	253.7	$Pa^{-1}s^{-1}$	(-485.6, 992.9)
β	0.5379	Pa^{-2}	(-6.972, 8.048)
γ	54.57	$Pa^{-1}s^{-1}$	(12.85, 96.28)
η	-63.96	s^{-1}	(-221.4, 93.5)
n	-3.612		(-39.64, 32.42)

Table 4.4: Fitted values of coefficients in relations (4.1a), (4.1b) and (4.1c) for the stress-controlled and rate-controlled data Boltenhagen et al. (1997b).

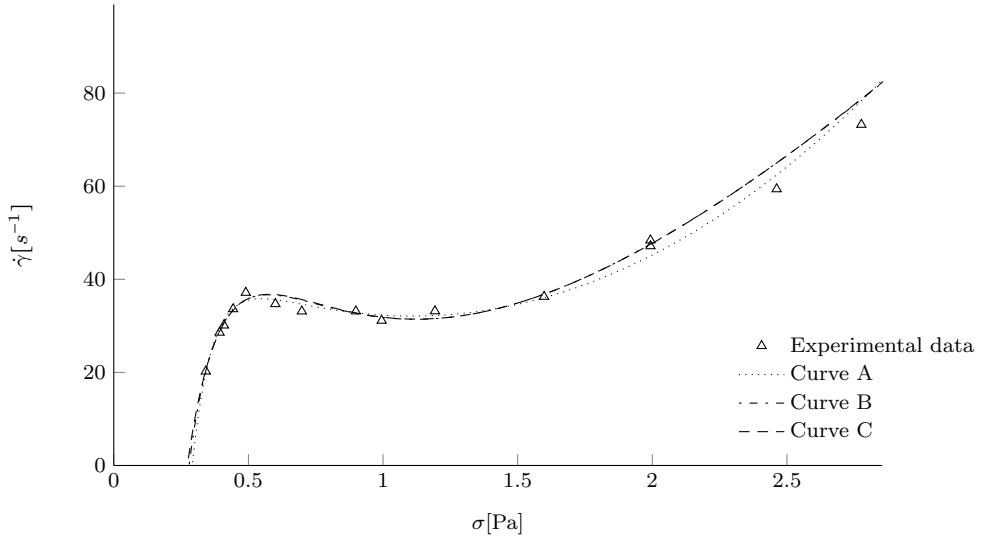

Figure 4.4: Fit of stress-controlled experimental data; Hu et al. (1998a).

Curve A

Coefficient	Fitted value	Unit	95% confidence bounds
a	-0.02092	Pa^{-1}	(-0.6874, 0.6456)
a_1	775.3	$\mathrm{s}^{-1}\mathrm{Pa}^{-1}$	$(-2.377 \times 10^4, 2.532 \times 10^4)$
a_2	-2089	s^{-1}	(-9379, 5201)
b	13.05	Pa^{-1}	(-11.33, 37.42)
b_1	-767.2	$\mathrm{s}^{-1}\mathrm{Pa}^{-1}$	$(-2.685 \times 10^4, 2.532 \times 10^4)$
b_2	2141	s^{-1}	(-5131, 9413)

Curve B

Coefficient	Fitted value	Unit	95% confidence bounds
p_1	65.15	$\mathrm{Pa}^{-1}\mathrm{s}^{-1}$	(35.42, 94.88)
p_2	-141.7	s^{-1}	(-239.5, -43.93)
p_3	156.4	Pas^{-1}	(39.27, 273.5)
p_4	-34.08	$\mathrm{Pa}^2\mathrm{s}^{-1}$	(-58.46, -9.689)
q_1	0.4388	Pa	(-0.3455, 1.223)
q_2	2.715×10^{-9}	Pa^2	(fixed at bound)

Curve C

Coefficient	Fitted value	Unit	95% confidence bounds
α	2030	$\mathrm{Pa}^{-1}\mathrm{s}^{-1}$	$(-8517, 1.258 \times 10^4)$
β	15.77	Pa^{-2}	(-56.43, 87.98)
γ	72.31	$\mathrm{Pa}^{-1}\mathrm{s}^{-1}$	(35.7, 108.9)
η	-349.8	s^{-1}	(-1738, 1038)
n	-0.6673		(-1.393, 0.05895)

Table 4.5: Fitted values of coefficients in relations (4.1a), (4.1b) and (4.1c) for the stress-controlled data Hu et al. (1998a). The value of the coefficient q_2 is bounded from below by 0.

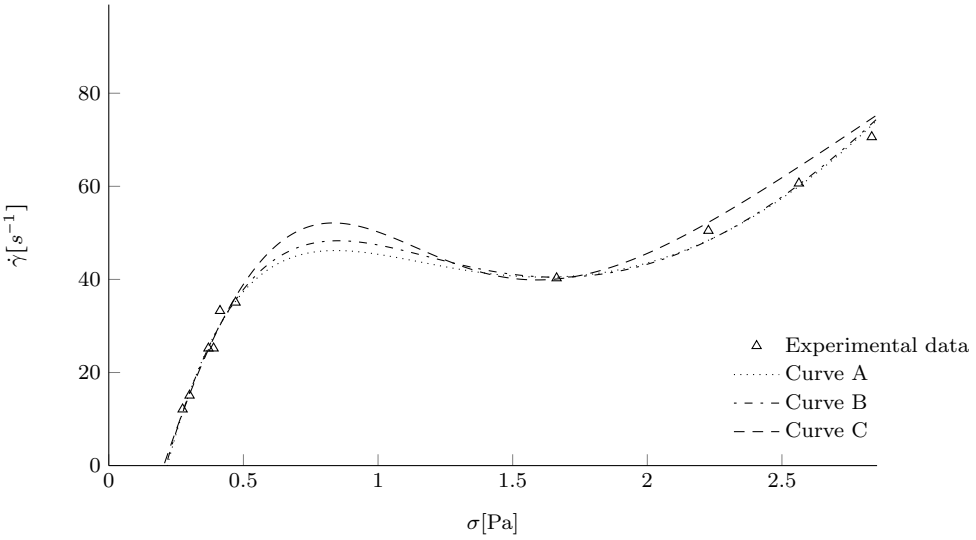

Figure 4.5: Fit of rate-controlled experimental data; Hu et al. (1998a).

Curve A

Coefficient	Fitted value	Unit	95% confidence bounds
a	-0.08992	Pa^{-1}	(-1.315, 1.135)
a_1	172.2	$s^{-1}Pa^{-1}$	(-2134, 2478)
a_2	-72.97	s^{-1}	(-237.1, 91.18)
b	2.177	Pa^{-1}	(-10.62, 14.97)
b_1	-213.8	$s^{-1}Pa^{-1}$	(-2310, 1883)
b_2	142.5	s^{-1}	(-738.3, 1023)

Curve B

Coefficient	Fitted value	Unit	95% confidence bounds
p_1	130.1	$Pa^{-1}s^{-1}$	(-356.9, 617.1)
p_2	-463	s^{-1}	(-2310, 1384)
p_3	627.7	Pas^{-1}	(-2202, 3457)
p_4	-113.6	Pa^2s^{-1}	(-662.6, 435.5)
q_1	0.8208	Pa	(-16.27, 17.91)
q_2	2.003	Pa^2	(-2.945, 6.95)

Curve C

Coefficient	Fitted value	Unit	95% confidence bounds
α	152	$Pa^{-1}s^{-1}$	(-52.73, 356.8)
β	0.04707	Pa^{-2}	(-2.241, 2.335)
γ	39.55	$Pa^{-1}s^{-1}$	(24.11, 54.98)
η	-37.61	s^{-1}	(-87.57, 12.35)
n	-24.95		(-1172, 1122)

Table 4.6: Fitted values of coefficients in relations (4.1a), (4.1b) and (4.1c) for the rate-controlled data Hu et al. (1998a).

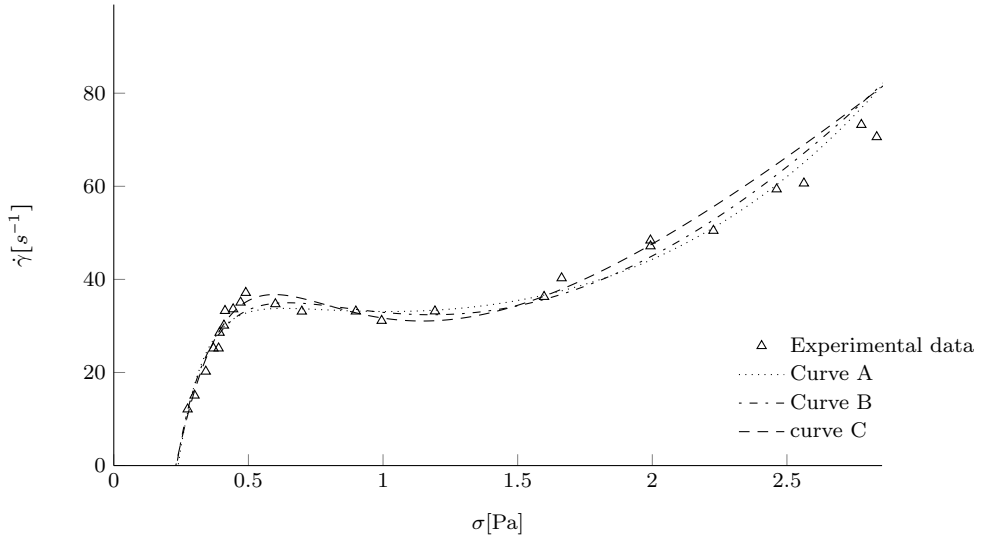

Figure 4.6: Fit of both the stress-controlled and the rate-controlled experimental data; Hu et al. (1998a).

Curve A

Coefficient	Fitted value	Unit	95% confidence bounds
a	-0.2911	Pa^{-1}	(-0.5111, -0.0711)
a_1	76.38	$\mathrm{s}^{-1}\mathrm{Pa}^{-1}$	(-47.69, 200.5)
a_2	-443.4	s^{-1}	(-1565, 678)
b	10.77	Pa^{-1}	(0.5275, 21.01)
b_1	40.38	$\mathrm{s}^{-1}\mathrm{Pa}^{-1}$	(-247.1, 327.9)
b_2	483.7	s^{-1}	(-617.7, 1585)

Curve B

Coefficient	Fitted value	Unit	95% confidence bounds
p_1	132.5	$\mathrm{Pa}^{-1}\mathrm{s}^{-1}$	(0.6651, 264.4)
p_2	-341.9	s^{-1}	(-741.6, 57.85)
p_3	440.8	Pas^{-1}	(-125.2, 1007)
p_4	-85.92	$\mathrm{Pa}^2\mathrm{s}^{-1}$	(-194.5, 22.67)
q_1	3.422	Pa	(-2.246, 9.089)
q_2	1.238×10^{-8}	Pa^2	(fixed at bound)

Curve C

Coefficient	Fitted value	Unit	95% confidence bounds
α	425.9	$\mathrm{Pa}^{-1}\mathrm{s}^{-1}$	(-160.6, 1013)
β	3.338	Pa^{-2}	(-3.451, 10.13)
γ	53.92	$\mathrm{Pa}^{-1}\mathrm{s}^{-1}$	(37.63, 70.2)
η	-92.77	s^{-1}	(-203.7, 18.13)
n	-1.225		(-2.503, 0.05221)

Table 4.7: Fitted values of coefficients in relations (4.1a), (4.1b) and (4.1c) for the stress-controlled and rate-controlled data Hu et al. (1998a). The value of the coefficient q_2 is bounded from below by 0.

5. Three-dimensional models of constitutive relations

So far, we have been investigating the one-dimensional relations between the component $\dot{\gamma}$ of the symmetric part of the velocity gradient $\mathbb{D}$ and the corresponding component σ of the Cauchy stress tensor $\mathbb{T}$. Now we will advance in the reasoning and we will try to develop the fully three-dimensional constitutive relations.

Typically, a constitutive relation is considered in the form so that the traceless part of the Cauchy stress tensor satisfies $\mathbb{T}_\delta = g(\mathbb{T}_\delta, \mathbb{D})\,\mathbb{D}$ where g is a scalar function. In this section, we will abandon this classical approach and we will take interest in a more general type $f(\mathbb{T}_\delta, \mathbb{D}) = 0$ where f is a tensorial function.

5.1 Conditions for constitutive relations

The construction of a constitutive relation is not a trivial problem. The suggested relation must have a specific form in order to fulfill several conditions.

Let us assume a general implicit form of the constitutive relation $f(\mathbb{T}, \mathbb{D}) = 0$ and let us ignore for simplicity the effects of the yield stress. The relations of this type then must satisfy the following conditions:

1. If we assume that the fluid is isotropic, the tensorial function f in the implicit relation is isotropic and according to the representation theorem it must have the following form

$$\begin{aligned}\alpha_0\mathbb{I} + \alpha_1\mathbb{T} + \alpha_2\mathbb{D} + \alpha_3\mathbb{T}^2 + \alpha_4\mathbb{D}^2 + \alpha_5\left(\mathbb{T}\mathbb{D} + \mathbb{D}\mathbb{T}\right) \\ + \alpha_6\left(\mathbb{T}^2\mathbb{D} + \mathbb{D}\mathbb{T}^2\right) + \alpha_7\left(\mathbb{T}\mathbb{D}^2 + \mathbb{D}^2\mathbb{T}\right) + \alpha_8\left(\mathbb{T}^2\mathbb{D}^2 + \mathbb{D}^2\mathbb{T}^2\right) = \mathbb{0}, \qquad (5.1)\end{aligned}$$

   where the coefficients α_i, $i = 0, \ldots, 8$ depend on the invariants of the tensors $\mathbb{T}$ and $\mathbb{D}$, see Rajagopal (2006) for details.

2. If we assume that the fluid is homogeneous and incompressible, the tensor $\mathbb{D}$ must fulfill the condition

$$\operatorname{Tr}\mathbb{D} = 0 \qquad (5.2)$$

   equivalent to the continuity equation (1.5).

3. The constitutive relation must be thermodynamically admissible, that is the second law of thermodynamics formulated as $\mathbb{T} : \mathbb{D} \geq 0$ must be satisfied.

4. The relation must be dynamically admissible. Provided that we are interested in simple shear flow geometry, see Section 1.3, the velocity field in the form

$\mathbf{v} = v^{\hat{z}}(y)\boldsymbol{e}_{\hat{z}}$ must be a solution to the governing equations and the constitutive relations.

5.2 Example of a constitutive relation

In this part, we will consider an incompressible fluid and the constitutive relation in the form

$$\alpha_1 \mathbb{T}_\delta + \alpha_2 \mathbb{D} + \alpha_3 \left(\mathbb{T}_\delta^2\right)_\delta = \mathbb{0}, \tag{5.3}$$

where the coefficients α_i, $i = 1, 2, 3$ depend on the invariants of $\mathbb{T}_\delta$ and $\mathbb{D}$.

As can be noticed, the relation was derived from the formula (5.1), assuming that $\alpha_0 = \alpha_4 = \alpha_5 = \alpha_6 = \alpha_7 = \alpha_8 = 0$ and taking the traceless parts of the tensors $\mathbb{T}$ and $\mathbb{T}_\delta^2$. If we make the trace of the both sides of the formula (5.3), we get the equation $\operatorname{Tr}\mathbb{D} = 0$ that is consistent with the fluid incompressibility. The relation can additionally be understood as the traceless counterpart of the formula that would be derived from the general constitutive relation (5.1) with the assumption $\alpha_0 = \alpha_4 = \alpha_5 = \alpha_6 = \alpha_7 = \alpha_8 = 0$.

Let us consider the simple shear flow geometry as shown in Figure **??**, where the velocity field has the form $\mathbf{v} = v^{\hat{z}}(y)\boldsymbol{e}_{\hat{z}}$. We will assume the Cauchy stress tensor in the form

$$\mathbb{T} = \begin{bmatrix} \mathrm{C} & 0 & 0 \\ 0 & \mathrm{C}+\mathrm{A} & \mathrm{T} \\ 0 & \mathrm{T} & \mathrm{C}+\mathrm{B} \end{bmatrix}, \tag{5.4}$$

where A, B, C and T are constants. Note that $\operatorname{Tr}\mathbb{T} = 3\mathrm{C}+\mathrm{A}+\mathrm{B}$, and that the traceless part of the tensor $\mathbb{T}$ takes the form

$$\mathbb{T}_\delta = \begin{bmatrix} -\frac{\mathrm{A}+\mathrm{B}}{3} & 0 & 0 \\ 0 & \frac{2\mathrm{A}-\mathrm{B}}{3} & \mathrm{T} \\ 0 & \mathrm{T} & \frac{2\mathrm{B}-\mathrm{A}}{3} \end{bmatrix}, \tag{5.5}$$

which is independent of C. Hence, the form of the Cauchy stress tensor is chosen in such a way that if $v^{\hat{z}}$ is identically zero, then the stress field automatically reduces to the spherical stress field $\mathbb{T} = \mathrm{C}\mathbb{I}$.

Let us now investigate the constitutive relation (5.3) in the simple shear flow setting, that is the velocity takes the form $\mathbf{v} = v^{\hat{z}}(y)\boldsymbol{e}_{\hat{z}}$ and the Cauchy stress tensor takes the form (5.4). First we express explicitly the individual components of the constitutive relation.

$$\mathbb{D} = \frac{1}{2}\frac{\mathrm{d}v^{\hat{z}}}{\mathrm{d}y}\begin{bmatrix} 0 & 0 & 0 \\ 0 & 0 & 1 \\ 0 & 1 & 0 \end{bmatrix}, \tag{5.6a}$$

$$(\mathbb{T}_\delta)^2 = \begin{bmatrix} \frac{(\mathrm{A}+\mathrm{B})^2}{9} & 0 & 0 \\ 0 & \frac{(2\mathrm{A}-\mathrm{B})^2}{9} + \mathrm{T}^2 & \frac{\mathrm{A}+\mathrm{B}}{3}\mathrm{T} \\ 0 & \frac{\mathrm{A}+\mathrm{B}}{3}\mathrm{T} & \frac{(2\mathrm{B}-\mathrm{A})^2}{9} + \mathrm{T}^2 \end{bmatrix}, \tag{5.6b}$$

$$\left((\mathbb{T}_\delta)^2\right)_\delta = \frac{1}{3}\begin{bmatrix} \frac{2(\mathrm{A}+\mathrm{B})^2-(2\mathrm{A}-\mathrm{B})^2-(2\mathrm{B}-\mathrm{A})^2}{9} - 2\mathrm{T}^2 & 0 & 0 \\ 0 & \frac{2(2\mathrm{A}-\mathrm{B})^2-(\mathrm{A}+\mathrm{B})^2-(2\mathrm{B}-\mathrm{A})^2}{9} + \mathrm{T}^2 & \frac{\mathrm{T}}{3}(\mathrm{A}+\mathrm{B}) \\ 0 & \frac{\mathrm{T}}{3}(\mathrm{A}+\mathrm{B}) & \frac{2(2\mathrm{B}-\mathrm{A})^2-(\mathrm{A}+\mathrm{B})^2-(2\mathrm{A}-\mathrm{B})^2}{9} + \mathrm{T}^2 \end{bmatrix}. \tag{5.6c}$$

The constitutive relation then takes the following form

$$\alpha_1\begin{bmatrix} -\frac{\mathrm{A}+\mathrm{B}}{3} & 0 & 0 \\ 0 & \frac{2\mathrm{A}-\mathrm{B}}{3} & \mathrm{T} \\ 0 & \mathrm{T} & \frac{2\mathrm{B}-\mathrm{A}}{3} \end{bmatrix} + \frac{\alpha_2}{2}\frac{\mathrm{d}v^{\hat{z}}}{\mathrm{d}y}\begin{bmatrix} 0 & 0 & 0 \\ 0 & 0 & 1 \\ 0 & 1 & 0 \end{bmatrix} + \frac{\alpha_3}{3}\begin{bmatrix} \mathrm{a}_{11} & 0 & 0 \\ 0 & \mathrm{a}_{22} & \mathrm{a}_{23} \\ 0 & \mathrm{a}_{32} & \mathrm{a}_{33} \end{bmatrix} = 0, \tag{5.7}$$

where

$$\mathrm{a}_{11} = \frac{2\left(\mathrm{A}+\mathrm{B}\right)^2 - \left(2\mathrm{A}-\mathrm{B}\right)^2 - \left(2\mathrm{B}-\mathrm{A}\right)^2}{9} - 2\mathrm{T}^2$$

$$\mathrm{a}_{22} = \frac{2\left(2\mathrm{A}-\mathrm{B}\right)^2 - \left(\mathrm{A}+\mathrm{B}\right)^2 - \left(2\mathrm{B}-\mathrm{A}\right)^2}{9} + \mathrm{T}^2$$

$$\mathrm{a}_{33} = \frac{2\left(2\mathrm{B}-\mathrm{A}\right)^2 - \left(\mathrm{A}+\mathrm{B}\right)^2 - \left(2\mathrm{A}-\mathrm{B}\right)^2}{9} + \mathrm{T}^2$$

and

$$\mathrm{a}_{23} = \mathrm{a}_{32} = \frac{\mathrm{T}}{3}\left(\mathrm{A}+\mathrm{B}\right).$$

The relation (5.7) leads to the following three scalar equations

$$-\alpha_1\frac{\mathrm{A}+\mathrm{B}}{3} + \alpha_3\left(\frac{2\left(\mathrm{A}+\mathrm{B}\right)^2 - \left(2\mathrm{A}-\mathrm{B}\right)^2 - \left(2\mathrm{B}-\mathrm{A}\right)^2}{27} - \frac{2}{3}\mathrm{T}^2\right) = 0, \tag{5.8a}$$

$$\alpha_1\frac{2\mathrm{A}-\mathrm{B}}{3} + \alpha_3\left(\frac{2\left(2\mathrm{A}-\mathrm{B}\right)^2 - \left(\mathrm{A}+\mathrm{B}\right)^2 - \left(2\mathrm{B}-\mathrm{A}\right)^2}{27} + \frac{\mathrm{T}^2}{3}\right) = 0, \tag{5.8b}$$

$$\alpha_1\frac{2\mathrm{B}-\mathrm{A}}{3} + \alpha_3\left(\frac{2\left(2\mathrm{B}-\mathrm{A}\right)^2 - \left(\mathrm{A}+\mathrm{B}\right)^2 - \left(2\mathrm{A}-\mathrm{B}\right)^2}{27} + \frac{\mathrm{T}^2}{3}\right) = 0, \tag{5.8c}$$

for the diagonal terms and to one equation

$$\alpha_1\mathrm{T} + \frac{\alpha_2}{2}\frac{\mathrm{d}v^{\hat{z}}}{\mathrm{d}y} + \alpha_3\frac{\mathrm{T}\left(\mathrm{A}+\mathrm{B}\right)}{9} = 0. \tag{5.8d}$$

for the only non-trivial off-diagonal term.

These equations are however not all independent. The constitutive relation (5.3) is constructed in such a way that the trace of the left hand side be zero. That implies that only two of the three equations involving the diagonal terms are independent. If

we notice the similarities between the equations (5.8b) and (5.8c), we can replace them by a the only one in the form

$$(\mathrm{A}-\mathrm{B})\left[\alpha_1+\alpha_3\frac{\mathrm{A}+\mathrm{B}}{3}\right]=0. \tag{5.8e}$$

that we constructed by the subtraction of (5.8c) from (5.8b). Finally, (5.8a), (5.8d) and (5.8e) form a system of three independent equations.

From the equation (5.8e), we can immediately deduce that either

$$\mathrm{A}=\mathrm{B} \tag{5.9}$$

or

$$\mathrm{A}+\mathrm{B}=-3\frac{\alpha_1}{\alpha_3}. \tag{5.10}$$

If we go back to the assumed form of the Cauchy stress tensor, see (5.4), we see that if $\mathrm{A}\neq 0$ and $\mathrm{B}\neq 0$ then (5.4) and (5.9) imply that

$$\mathrm{T}_{\hat{x}\hat{x}}-\mathrm{T}_{\hat{z}\hat{z}}\neq 0, \tag{5.11a}$$

and

$$\mathrm{T}_{\hat{y}\hat{y}}-\mathrm{T}_{\hat{z}\hat{z}}=0. \tag{5.11b}$$

On the other hand, (5.4) and (5.10) imply that

$$\mathrm{T}_{\hat{x}\hat{x}}-\mathrm{T}_{\hat{z}\hat{z}}\neq 0, \tag{5.12a}$$

and

$$\mathrm{T}_{\hat{y}\hat{y}}-\mathrm{T}_{\hat{z}\hat{z}}\neq 0. \tag{5.12b}$$

The investigated model is therefore interesting from the point of modelling normal stress differences effect, see Schowalter (1978) for more details.

5.3 Thermodynamical admissibility for $\mathrm{A}+\mathrm{B}=-3\frac{\alpha_1}{\alpha_3}$

We will investigate the conditions of the thermodynamical admissibility for the constitutive relation $\alpha_1\mathbb{T}_\delta+\alpha_2\mathbb{D}+\alpha_3\left(\mathbb{T}_\delta^2\right)_\delta=\mathbb{0}$ if (5.8e) reduces to

$$\mathrm{A}+\mathrm{B}=-3\frac{\alpha_1}{\alpha_3}. \tag{5.13}$$

If the relation (5.13) holds, the equations (5.8d) and (5.8a) can be written respectively in the forms

$$\mathrm{T}=-\frac{3}{4}\frac{\alpha_2}{\alpha_1}\frac{\mathrm{d}v^{\hat{z}}}{\mathrm{d}y} \tag{5.14}$$

and

$$(\mathrm{A}-\mathrm{B})^2=9\left(\frac{\alpha_1^2}{\alpha_3^2}-\frac{1}{4}\frac{\alpha_2^2}{\alpha_1^2}\left(\frac{\mathrm{d}v^{\hat{z}}}{\mathrm{d}y}\right)^2\right). \tag{5.15}$$

Let us now define a relation between the coefficients α_1, α_2 and α_3

$$\alpha_3=_{\mathrm{def}}\frac{\alpha_1^2}{\alpha_2}\frac{1}{\left|\frac{\mathrm{d}v^{\hat{z}}}{\mathrm{d}y}\right|}\beta, \tag{5.16}$$

where β is a constant. If we substitute this formula into (5.15), we get the equation in the form

$$(\mathrm{A}-\mathrm{B})^2 = 9\frac{\alpha_2^2}{\alpha_1^2}\left(\frac{1}{\beta^2}-\frac{1}{4}\right)\left(\frac{\mathrm{d}v^{\hat{z}}}{\mathrm{d}y}\right)^2. \tag{5.17}$$

It is evident that the right hand side of this expression has to be positive. That implies that the coefficient β has to satisfy the condition $\beta^2 < 4$.

Summarizing our partial results, we can rewrite the original system (5.8a), (5.8d) and (5.8e) in the reduced form

$$\mathrm{A}+\mathrm{B} = -3\frac{\alpha_2}{\alpha_1}\frac{1}{\beta}\left|\frac{\mathrm{d}v^{\hat{z}}}{\mathrm{d}y}\right|, \tag{5.18a}$$

$$(\mathrm{A}-\mathrm{B})^2 = 9\frac{\alpha_2^2}{\alpha_1^2}\left(\frac{1}{\beta^2}-\frac{1}{4}\right)\left(\frac{\mathrm{d}v^{\hat{z}}}{\mathrm{d}y}\right)^2, \tag{5.18b}$$

$$\mathrm{T} = -\frac{3}{4}\frac{\alpha_2}{\alpha_1}\frac{\mathrm{d}v^{\hat{z}}}{\mathrm{d}y}. \tag{5.18c}$$

Let us now focus on the thermodynamical admissibility of the relation (5.3) that is generally expressed as

$$\mathbb{T}:\mathbb{D} \geq 0. \tag{5.19}$$

In the examined relation (5.3) the tensor $\mathbb{D}$ is traceless so the requirement on the admissibility (5.19) is equivalent to

$$\mathbb{T}_\delta:\mathbb{D} \geq 0. \tag{5.20}$$

Multiplying (5.3) by $\mathbb{D}$ leads to

$$\alpha_1\mathbb{T}:\mathbb{D} + \alpha_2\mathbb{D}:\mathbb{D} + \alpha_3\left(\mathbb{T}_\delta^2\right):\mathbb{D} = \mathbb{0}. \tag{5.21}$$

If we substitute the coefficient α_3 expressed in the form (5.16) into the relation (5.21) we get the expression for $\mathbb{T}:\mathbb{D}$ in the form

$$\mathbb{T}:\mathbb{D} = -\frac{\alpha_2}{\alpha_1}\mathbb{D}:\mathbb{D} - \frac{\alpha_1}{\alpha_2}\frac{\beta}{\sqrt{2}\,|\mathbb{D}|}\left(\mathbb{T}^2{}_\delta\right):\mathbb{D}. \tag{5.22}$$

Assuming that $\beta > 0$, $\alpha_1 > 0$, $\alpha_2 < 0$ and introducing the coefficient $\widetilde{\alpha}_2 =_{\mathrm{def}} -\alpha_2$, we can make the following estimates on the right hand side of the expression (5.22)

$$\mathbb{T}:\mathbb{D} = \frac{\widetilde{\alpha}_2}{\alpha_1}\left(\mathbb{D}:\mathbb{D} + \frac{\alpha_1^2}{\widetilde{\alpha}_2^2}\frac{\beta}{\sqrt{2}\,|\mathbb{D}|}\mathbb{T}_\delta^2:\mathbb{D}\right) \geq \frac{\widetilde{\alpha}_2}{\alpha_1}\left(\mathbb{D}:\mathbb{D} - \frac{\alpha_1^2}{\widetilde{\alpha}_2^2}\frac{\beta}{\sqrt{2}\,|\mathbb{D}|}\left|\mathbb{T}_\delta^2:\mathbb{D}\right|\right), \tag{5.23}$$

$$\geq \frac{\widetilde{\alpha}_2}{\alpha_1}\left(|\mathbb{D}|^2 - \frac{\alpha_1^2}{\widetilde{\alpha}_2^2}\frac{\beta}{\sqrt{2}}|\mathbb{T}_\delta|^2\right) \tag{5.24}$$

where we have used the Cauchy-Schwartz inequality, $|\mathbb{A}:\mathbb{B}| \leq |\mathbb{A}|\,|\mathbb{B}|$.
Defining the relation between the coefficients α_1 and $\widetilde{\alpha}_2$ as follows

$$\frac{\alpha_1^2}{\widetilde{\alpha}_2^2}\frac{\beta}{\sqrt{2}} =_{\mathrm{def}} \gamma\frac{|\mathbb{D}|^2}{|\mathbb{T}_\delta|^2}, \tag{5.25}$$

where the coefficient γ can be a function of the invariants of $\mathbb{D}$ and $\mathbb{T}_\delta$, the inequality (5.24) can be rewritten in the form

$$\mathbb{T}:\mathbb{D} \geq \frac{\widetilde{\alpha}_2}{\alpha_1}(1-\gamma)\,|\mathbb{D}|^2. \tag{5.26}$$

The requirement of the thermodynamical admissibility is then satisfied for $\gamma \in [0,1]$. Assuming the defined relations (5.16) and (5.25) between the coefficients α_1, α_2 and α_3, a thermodynamical admissible constitutive relation takes the form

$$\left(\frac{\gamma\sqrt{2}}{\beta}\right)^{\frac{1}{2}} |\mathbb{D}|\,|\mathbb{T}_\delta|\,\mathbb{T}_\delta - \mathbb{D}\,|\mathbb{T}_\delta|^2 - \gamma\,|\mathbb{D}|\left(\mathbb{T}_\delta^2\right)_\delta = 0, \tag{5.27}$$

where $\gamma \in [0,1]$ and $0 < \beta < 2$.

5.4 Dynamical admissibility for $\mathrm{A} + \mathrm{B} = -3\frac{\alpha_1}{\alpha_3}$

According to the results of the previous section, the sufficient conditions for the thermodynamical admissibility of the constitutive relation (5.3) are the restrictions on the coefficients γ and β: $\gamma \in [0,1]$, $0 < \beta < 2$. Let us now investigate whether exists a dynamical admissible solution to the system (5.18), consistent with these conditions.

The norm of the traceless part of the Cauchy stress tensor can be expressed as

$$|\mathbb{T}_\delta| = \left(\frac{(\mathrm{A}+\mathrm{B})^2 + (2\mathrm{A}-\mathrm{B})^2 + (2\mathrm{B}-\mathrm{A})^2}{9} + 2\mathrm{T}^2\right)^{\frac{1}{2}} = \left(\frac{(\mathrm{A}+\mathrm{B})^2}{6} + \frac{(\mathrm{A}-\mathrm{B})^2}{2} + 2\mathrm{T}^2\right)^{\frac{1}{2}}. \tag{5.28}$$

Substituting the equations (5.18) into the formula (5.28), we get the following relation

$$|\mathbb{T}_\delta|^2 = 6\frac{\widetilde{\alpha}_2^2}{\alpha_1^2}\left(\frac{\mathrm{d}v^{\hat{z}}}{\mathrm{d}y}\right)^2 \frac{1}{\beta^2}. \tag{5.29}$$

Using the relation (5.25), we can rewrite the formula (5.29) as

$$|\mathbb{T}_\delta|^2 = \frac{12}{\gamma\beta\sqrt{2}}\,|\mathbb{T}_\delta|^2, \tag{5.30}$$

which implies

$$\gamma = \frac{12}{\beta\sqrt{2}}. \tag{5.31}$$

As can be seen from (5.31), the sufficient condition for the thermodynamical stability cannot be consistent with this result that is issued from our analysis of the dynamical stability. If $\gamma \in [0,1]$, the coefficient β cannot take the values from the interval $(0,2)$.

5.5 Thermodynamical admissibility for $\mathrm{A} = \mathrm{B}$

One of the relations between A and B that are implied from the equation (5.8e) is $\mathrm{A} = \mathrm{B}$. Holding this equality, the equations (5.8a) and (5.8d) take the forms respectively

$$-\frac{2}{3}\alpha_1\mathrm{A} + \frac{2}{9}\alpha_3\mathrm{A}^2 - \frac{2}{3}\alpha_3\mathrm{T}^2 = 0, \tag{5.32a}$$

$$\alpha_1\mathrm{T} + \frac{\alpha_2}{2}\frac{\mathrm{d}v^{\hat{z}}}{\mathrm{d}y} + \frac{2}{9}\alpha_3\mathrm{TA} = 0. \tag{5.32b}$$

Solving the equation (5.32a) for A, we always get a real solution

$$\mathrm{A} = \frac{2}{3}\left(\frac{\alpha_1}{\alpha_3} \pm \sqrt{\left(\frac{\alpha_1}{\alpha_3}\right)^2 + \frac{4}{3}\mathrm{T}^2}\right). \tag{5.33}$$

This fact prevent us from making restrictions on the coefficients α_1 and α_3, unlike in the previous case for $A + B = -3\frac{\alpha_1}{\alpha_3}$.

Let us now make an analysis of the thermodynamical admissibility of the relation $\alpha_1 \mathbb{T}_\delta + \alpha_2 \mathbb{D} + \alpha_3 \left(\mathbb{T}_\delta^2\right)_\delta = \mathbb{0}$ with A = B and let us verify if the general requirement for the thermodynamical stability (5.19) is satisfied for some values of the coefficients α_1, α_2 and α_3.

We multiply the relation by $\mathbb{D}$

$$\alpha_1 \mathbb{T} : \mathbb{D} + \alpha_2 \mathbb{D} : \mathbb{D} + \alpha_3 \mathbb{T}_\delta^2 : \mathbb{D} = \mathbb{0}. \tag{5.34}$$

Separating the term $\mathbb{T} : \mathbb{D}$, we get the relation

$$\mathbb{T} : \mathbb{D} = -\frac{\alpha_2}{\alpha_1} \left(\mathbb{D} : \mathbb{D} + \frac{\alpha_3}{\alpha_2} \left(\mathbb{T}_\delta^2 \right) : \mathbb{D} \right). \tag{5.35}$$

Assuming the following restrictions on the coefficients

$$\alpha_1 > 0, \tag{5.36a}$$

$$\alpha_2 < 0, \tag{5.36b}$$

$$\alpha_3 > 0, \tag{5.36c}$$

and defining $\widetilde{\alpha}_2 =_{\text{def}} -\alpha_2$, we can make the following estimates on the right hand side of (5.35)

$$\mathbb{T} : \mathbb{D} = \frac{\widetilde{\alpha}_2}{\alpha_1} \left(\mathbb{D} : \mathbb{D} - \frac{\alpha_3}{\widetilde{\alpha}_2} \mathbb{T}_\delta^2 : \mathbb{D} \right) \geq \frac{\widetilde{\alpha}_2}{\alpha_1} \left(\mathbb{D} : \mathbb{D} - \frac{\alpha_3}{\widetilde{\alpha}_2} \left| \mathbb{T}_\delta^2 : \mathbb{D} \right| \right) \geq \frac{\widetilde{\alpha}_2}{\alpha_1} \left(|\mathbb{D}|^2 - \frac{\alpha_3}{\widetilde{\alpha}_2} |\mathbb{T}_\delta|^2 |\mathbb{D}| \right). \tag{5.37}$$

If we define the relation between the coefficients α_3 and $\widetilde{\alpha}_2$ as

$$\frac{\alpha_3}{\widetilde{\alpha}_2} =_{\text{def}} \gamma \frac{|\mathbb{D}|}{|\mathbb{T}_\delta|^2}, \tag{5.38}$$

we can rewrite the inequality (5.37) in the form

$$\mathbb{T}_\delta : \mathbb{D} \geq \frac{\widetilde{\alpha}_2}{\alpha_1} (1 - \gamma) |\mathbb{D}|^2. \tag{5.39}$$

As in the previous case, the condition of the thermodynamical admissibility (5.19) is fulfilled for $\gamma \in [0, 1]$.

5.6 Dynamical admissibility for A = B

In the previous section, we showed that the sufficient conditions for the thermodynamical admissibility of the constitutive relation (5.3) with A=B are that the coefficients α_1, α_2 and α_3 fulfill the conditions (5.36) and that for the relation between the coefficients α_3 and $\widetilde{\alpha}_2$ defined as (5.38), the coefficient γ fulfills $\gamma \in [0, 1]$. Note that the coefficients α_1, α_2, α_3 and γ are assumed to be functions only of the invariants of $\mathbb{D}$ and $\mathbb{T}_\delta$. Hence, the system (5.32) is a system of implicit equations for A and T. We will now investigate whether exists a solution to this system, consistent with the derived thermodynamical admissibility conditions.

Recall that the norm of the traceless part of the Cauchy stress tensor can be expressed in the form

$$|\mathbb{T}_\delta| = \left(\frac{(A + B)^2}{6} + \frac{(A - B)^2}{2} + 2T^2 \right)^{\frac{1}{2}}. \tag{5.40}$$

For A=B this expression reduces to

$$|\mathbb{T}_\delta| = \sqrt{2}\left(\frac{\mathrm{A}^2}{3} + \mathrm{T}^2\right)^{\frac{1}{2}}. \tag{5.41}$$

Let us assume that α_3 is a constant. The dependence of the ratio $\frac{\alpha_3}{\widetilde{\alpha}_2}$ on $|\mathbb{D}|$ and on $|\mathbb{T}_\delta|$ is then due only to the dependence of the coefficient $\widetilde{\alpha}_2$ on these two invariants. The system (5.32) then reduces to

$$\mathrm{A}^2 - 3\frac{\alpha_1}{\alpha_3}\mathrm{A} - 3\mathrm{T}^2 = 0, \tag{5.42a}$$

$$\frac{\alpha_1}{\alpha_3}\mathrm{T} - \frac{1}{2}\frac{|\mathbb{T}_\delta|^2}{\gamma\,|\mathbb{D}|}\frac{\mathrm{d}v^{\hat{z}}}{\mathrm{d}y} + \frac{2}{9}\mathrm{TA} = 0. \tag{5.42b}$$

Substituting (5.41) into (5.42), the system (5.42) can be rewritten as

$$\mathrm{A}^2 - 3\frac{\alpha_1}{\alpha_3}\mathrm{A} - 3\mathrm{T}^2 = 0, \tag{5.43a}$$

$$\frac{\alpha_1}{\alpha_3}\mathrm{T} - \frac{\left(\frac{\mathrm{A}^2}{3} + \mathrm{T}^2\right)}{\frac{1}{\sqrt{2}}\gamma\left|\frac{\mathrm{d}v^{\hat{z}}}{\mathrm{d}y}\right|}\frac{\mathrm{d}v^{\hat{z}}}{\mathrm{d}y} + \frac{2}{9}\mathrm{TA} = 0. \tag{5.43b}$$

To simplify the form of this system (5.43), we define auxiliary coefficients u and v as

$$u =_{\mathrm{def}} \frac{\alpha_1}{\alpha_3}, \tag{5.44a}$$

$$v =_{\mathrm{def}} \frac{\sqrt{2}}{\gamma}\mathrm{sign}\left(\frac{\mathrm{d}v^{\hat{z}}}{\mathrm{d}y}\right). \tag{5.44b}$$

The system (5.43) then takes the form

$$\mathrm{A}^2 - 3u\mathrm{A} - 3\mathrm{T}^2 = 0, \tag{5.45a}$$

$$-v\mathrm{T}^2 + \left(\frac{2}{9}\mathrm{A} + u\right)\mathrm{T} - \frac{v}{3}\mathrm{A}^2 = 0. \tag{5.45b}$$

At given u and v (corresponding to the shear rate-controlled type of measurement), the system (5.45) is a system of equations for A and T. Since the two equations represent the equations of conics, the solution to the system is equivalent to the points of their intersection. Apparently, the equation (5.45a) describes a hyperbola and the equation (5.45b) describes an ellipse; both of them including the point (A = 0, T = 0). Performing analysis of the derivatives in this point, we realize that the line described by the equation A = 0 is tangent to the hyperbola whereas the line T = 0 is tangent to the ellipse. Therefore, for each given u and v, there exists a point of intersection of the two conics, hence there exists a real solution to the system (5.45).

Recall that one of the sufficient conditions for the thermodynamical admissibility is that the coefficient γ satisfies $\gamma \in [0, 1]$. There is however no limitation on its functional parameters, hence γ can be the function of $\frac{\mathrm{d}v^{\hat{z}}}{\mathrm{d}y}$. As an example of γ satisfying this conditions, we can choose

$$\gamma =_{\mathrm{def}} \frac{|\mathbb{D}|}{\sqrt{1 + \delta\,|\mathbb{D}|^2}}, \tag{5.46}$$

where $\delta > 1$ is a constant.

A thermodynamically and dynamically admissible implicit constitutive relation then can be written in the form

$$\frac{\alpha_1}{\alpha_3}\mathbb{T}_\delta - \frac{\left|\mathbb{T}_\delta^2\right|\sqrt{1+\delta\left|\mathbb{D}\right|^2}}{\left|\mathbb{D}\right|^2}\mathbb{D} + \left(\mathbb{T}_\delta^2\right)_\delta = 0. \tag{5.47}$$

Conclusion

In this work, we have demonstrated the utility of implicit constitutive relations in description of the behavior of some complex fluids and we have proposed a simple example of a fully three-dimensional implicit constitutive relation involving the normal stress differences effect.

The starting point of the work was a complex literature search. This search was focused on materials that exhibit a backward bending shear stress-shear rate curve and represent therefore the candidates to demonstrate the applicability of implicit constitutive relations. The search resulted in two classes of fluids: colloidal suspensions and surfactant solutions. As shown in literature, the backward bending character of flow curves was present only in the stress-controlled type of measurements. The rate-controlled type resulted particularly in a curve discontinuity without the bending region. The question why a fluid exhibits such an untypical behavior was examined by summarizing the principal existing microscopic theories on this topic. We have focused on the phenomena of the shear-thickening, the shear-thinning and the shear banding that form together a complete toolbox for the understanding of microscopic processes arising in the concerned fluid. Induced from the theories, a summarizing interpretation of the S-shaped shear stress-shear rate dependence can be expressed as follows. At specific imposed shear stress, the fluid separates in two bands of which one is constituted by the original fluid and the other is a shear-induced state. The bands have different structure, viscosity and shear rate (in the gradient banding) or shear stress (in the vorticity banding). As long as the fluid is separated in bands, the corresponding shear stress-shear rate curve displays the slightly bending behavior. The nature of the shear-induced band is approached by the presented shear-thickening and the shear-thinning theories.

The sets of extracted experimental data from the literature have been subsequently fitted by three constitutive relations of the type $\dot{\gamma} = f(\sigma)$. These have been proposed in such a way that they fit the specific shape of experimental curves. The one-dimensional relations can be understood as reduced forms of fully three-dimensional relations of the type $\mathbb{D} = g(\mathbb{T})$.

In the last section, we have been investigating constitutive relations of the type $\alpha_1 \mathbb{T}_\delta + \alpha_2 \mathbb{D} + \alpha_3 \left(\mathbb{T}_\delta^2\right)_\delta = \mathbb{0}$ with focus on discussion of normal stress differences effect. We have found the concrete expression of the coefficients α_1, α_2 and α_3 so that the relation fulfills the conditions required on a constitutive relation. The constructed relation has been found in the form

$$\frac{\alpha_1}{\alpha_3}\mathbb{T}_\delta - \frac{\left|\mathbb{T}_\delta^2\right|\sqrt{1+\delta\left|\mathbb{D}\right|^2}}{\left|\mathbb{D}\right|^2}\mathbb{D} + \left(\mathbb{T}_\delta^2\right)_\delta = 0. \tag{5.48}$$

Bibliography

Barentin, C. and A. J. Liu (2001). Shear thickening in dilute solutions of wormlike micelles. *EPL (Europhysics Letters) 55*(3), 432.

Bender, J. and N. J. Wagner (1996). Reversible shear thickening in monodisperse and bidisperse colloidal dispersions. *Journal of Rheology (1978-present) 40*(5).

Bertrand, E., J. Bibette, and V. Schmitt (2002, Dec). From shear thickening to shear-induced jamming. *Phys. Rev. E 66*, 060401.

Boltenhagen, P., Y. Hu, E. F. Matthys, and D. J. Pine (1997a). Inhomogeneous structure formation and shear-thickening in worm-like micellar solutions. *EPL (Europhysics Letters) 38*(5), 389.

Boltenhagen, P., Y. Hu, E. F. Matthys, and D. J. Pine (1997b, Sep). Observation of bulk phase separation and coexistence in a sheared micellar solution. *Phys. Rev. Lett. 79*, 2359–2362.

Brady, J. F. and G. Bossis (1985, 6). The rheology of concentrated suspensions of spheres in simple shear flow by numerical simulation. *Journal of Fluid Mechanics 155*, 105–129.

Brown, E. and H. M. Jaeger (2009, Aug). Dynamic jamming point for shear thickening suspensions. *Phys. Rev. Lett. 103*, 086001.

Bruinsma, R., W. M. Gelbart, and A. BenShaul (1992). Flowinduced gelation of living micellar polymers. *The Journal of Chemical Physics 96*.

Cates, M. E. and S. J. Candau (1990). Statics and dynamics of worm-like surfactant micelles. *Journal of Physics: Condensed Matter 2*(33), 6869.

Cates, M. E. and S. J. Candau (2001). Ring-driven shear thickening in wormlike micelles? *EPL (Europhysics Letters) 55*(6), 887.

Cates, M. E. and S. M. Fielding (2007, February). Rheology of giant micelles. *eprint arXiv:cond-mat/0702047*.

Cates, M. E. and M. S. Turner (1990). Flow-induced gelation of rodlike micelles. *EPL (Europhysics Letters) 11*(7), 681.

Cates, M. E., J. P. Wittmer, J.-P. Bouchaud, and P. Claudin (1998, Aug). Jamming, force chains, and fragile matter. *Phys. Rev. Lett. 81*, 1841–1844.

Cheng, X., J. H. McCoy, J. N. Israelachvili, and I. Cohen (2011). Imaging the microscopic structure of shear thinning and thickening colloidal suspensions. *Science 333*(6047), 1276–1279.

Chow, M. K. and C. F. Zukoski (1995). Nonequilibrium behavior of dense suspensions of uniform particles: Volume fraction and size dependence of rheology and microstructure. *Journal of Rheology (1978-present) 39*(1).

Dehmoune, J., J. P. Decruppe, O. Greffier, H. Xu, and P. Lindner (2009). Shear thickening in three surfactants of the alkyl family cntab: Small angle neutron scattering and rheological study. *Langmuir 25*(13), 7271–7278. PMID: 19492782.

Diat, O., D. Roux, and F. Nallet (1993). Effect of shear on a lyotropic lamellar phase. *Journal de Physique II 3*(9), 1427–1452.

Fagan, M. E. and C. F. Zukoski (1997). The rheology of charge stabilized silica suspensions. *Journal of Rheology (1978-present) 41*(2).

Förster, S., M. Konrad, and P. Lindner (2005, Jan). Shear thinning and orientational ordering of wormlike micelles. *Phys. Rev. Lett. 94*, 017803.

Ganguli, A. K., A. Ganguly, and S. Vaidya (2010). Microemulsion-based synthesis of nanocrystalline materials. *Chem. Soc. Rev. 39*, 474–485.

Goveas, J. and P. Olmsted (2001). A minimal model for vorticity and gradient banding in complex fluids. *The European Physical Journal E 6*(1), 79–89.

Hartmann, V. and R. Cressely (1997). Simple salts effects on the characteristics of the shear thickening exhibited by an aqueous micellar solution of ctab/nasal. *EPL (Europhysics Letters) 40*(6), 691.

Head, D. A., A. Ajdari, and M. E. Cates (2001, Nov). Jamming, hysteresis, and oscillation in scalar models for shear thickening. *Phys. Rev. E 64*, 061509.

Hoffman, R. (1974). Discontinuous and dilatant viscosity behavior in concentrated suspensions. ii. theory and experimental tests. *Journal of Colloid and Interface Science 46*(3), 491 – 506.

Hoffman, R. L. (1972). Discontinuous and dilatant viscosity behavior in concentrated suspensions. i. observation of a flow instability. *Transactions of The Society of Rheology (1957-1977) 16*(1).

Hoffman, R. L. (1998). Explanations for the cause of shear thickening in concentrated colloidal suspensions. *Journal of Rheology (1978-present) 42*(1).

Hu, Y., P. Boltenhagen, E. F. Matthys, and D. J. Pine (1998a). Shear thickening in low-concentration solutions of wormlike micelles. I. direct visualization of transient behavior and phase transitions. *Journal of Rheology*.

Hu, Y., P. Boltenhagen, E. F. Matthys, and D. J. Pine (1998b, Sep). Shear thickening in low-concentration solutions of wormlike micelles. II. slip, fracture, and stability of the shear-induced phase. *Journal of rheology*.

Keller, S. L., P. Boltenhagen, D. J. Pine, and J. A. Zasadzinski (1998, Mar). Direct observation of shear-induced structures in wormlike micellar solutions by freeze-fracture electron microscopy. *Phys. Rev. Lett. 80*, 2725–2728.

Lange, K. R. (1999). *Surfactants: A Practical Handbook*. Hanser Gardner Publications.

Liu, A. J. and S. R. Nagel (1998, Nov 05). Nonlinear dynamics: Jamming is not just cool any more. *Nature 396*(6706), 21–22.

Liu, C.-h. and D. J. Pine (1996, Sep). Shear-induced gelation and fracture in micellar solutions. *Phys. Rev. Lett. 77*, 2121–2124.

Lopez-Diaz, D., E. Sarmiento-Gomez, C. Garza, and R. Castillo (2010). A rheological study in the dilute regime of the worm-micelle fluid made of zwitterionic surfactant (tdps), anionic surfactant (sds), and brine. *Journal of Colloid and Interface Science 348*(1), 152 – 158.

Macias, E., A. Gonzalez, O. Manero, R. Gonzales-Nunez, J. Soltero, and P. Attané (2001). Flow regimes of dilute surfactant solutions. *Journal of Non-Newtonian Fluid Mechanics 101*(1–3), 149 – 172.

Mewis, J. and N. Wagner (2012). *Colloidal Suspension Rheology*. Cambridge University Press.

Málek, J., V. Průša, and K. R. Rajagopal (2010). Generalizations of the navier–stokes fluid from a new perspective. *International Journal of Engineering Science 48*(12), 1907 – 1924.

Olmsted, P. (2008). Perspectives on shear banding in complex fluids. *Rheologica Acta 47*(3), 283–300.

Paine, H. (1912). Kolloid-z., 2,115 (1912). *Kolloidchem. Beih 4*, 24.

Průša, V. and K. R. Rajagopal (2012). On implicit constitutive relations for materials with fading memory. *Journal of Non-Newtonian Fluid Mechanics 181–182*(0), 22 – 29.

Rajagopal, K. (2003). On implicit constitutive theories. *Applications of Mathematics 48*(4), 279–319.

Rajagopal, K. and A. Srinivasa (2008). On the thermodynamics of fluids defined by implicit constitutive relations. *Zeitschrift für angewandte Mathematik und Physik 59*(4), 715–729.

Rajagopal, K. R. (2006, 3). On implicit constitutive theories for fluids. *Journal of Fluid Mechanics 550*, 243–249.

Rangel-Yagui, C. O., A. Pessoa-Jr, and D. Blankschtein (2004, 12). Two-phase aqueous micellar systems: an alternative method for protein purification. *Brazilian Journal of Chemical Engineering 21*, 531 – 544.

Roux, D., F. Nallet, and O. Diat (1993). Rheology of lyotropic lamellar phases. *EPL (Europhysics Letters) 24*(1), 53.

Schowalter, W. (1978). *Mechanics of Non-Newtonian Fluids*. Pergamon Press.

Sollich, P., F. m. c. Lequeux, P. Hébraud, and M. E. Cates (1997, Mar). Rheology of soft glassy materials. *Phys. Rev. Lett. 78*, 2020–2023.

Sung, K., M. S. Han, and C. Kim (2003). Rheological behavior and wall slip of dilute and semidilute cpycl/nasal surfactant solutions. *journal vol. 15*(issue 3), 151–156.

Wang, S. Q. (1992). Transient network theory for shear-thickening fluids and physically crosslinked networks. *Macromolecules 25*(25), 7003–7010.

Wilkins, G. M. H. and P. D. Olmsted (2006). Vorticity banding during the lamellar-to-onion transition in a lyotropic surfactant solution in shear flow. *European Physical Journal E – Soft Matter 21*(2), 133 – 143.